Mon. Not. R. Astron. Soc. **000**, 000–000 (0000) Printed 2 February 2008 (MN LATEX style file v2.2)

Supernova 2002bo: inadequacy of the single parameter description.

S. Benetti[1], P. Meikle[2], M. Stehle[3,4], G. Altavilla[1], S. Desidera[1], G. Folatelli[5], A. Goobar[5], S. Mattila[6], J. Mendez[7], H. Navasardyan[1], A. Pastorello[1], F. Patat[8], M. Riello[1], P. Ruiz-Lapuente[3,7], D. Tsvetkov[9], M. Turatto[1], P. Mazzali[10,3] and W. Hillebrandt[3],

[1] *INAF - Osservatorio Astronomico di Padova, vicolo dell'Osservatorio 5, I-35122 Padova, Italy*
[2] *Blackett Laboratory, Imperial College London, Prince Consort Road, London, SW7 2BW United Kingdom*
[3] *Max-Planck-Institut für Astrophysik, P.O. Box 1317 D-85741 Garching, Germany*
[4] *Universitäts-Sternwarte München, Scheinerstr. 1, D-81679 München, Germany*
[5] *Department of Physics, Stockholm University, AlbaNova University Center, SE–106 91 Stockholm, Sweden*
[6] *Stockholm Observatory, Department of Astronomy, AlbaNova University Center, SE–106 91 Stockholm, Sweden*
[7] *Department of Astronomy, University of Barcelona, Marti i Franques 1, E-08028 Barcelona Spain*
[8] *European Southern Observatory, Karl-Schwarzschild-Str. 2, D-85748 Garching bei München, Germany*
[9] *Sternberg Astronomical Institute, Moscow University, Univeritetskii pr. 13, Moscow, 119992, Russia*
[10] *INAF - Osservatorio Astronomico di Trieste, Via Tiepolo, 11, I-34131 Trieste, Italy*

Received .....; accepted .....

ABSTRACT

We present optical/near-infrared photometry and spectra of the type Ia SN 2002bo spanning epochs from –13 days before maximum B-band light to +102 days after. The pre-maximum optical coverage is particularly complete. The extinction deduced from the observed colour evolution and from interstellar NaID absorption is quite high viz. $\mathrm{E}(B-V) = 0.43 \pm 0.10$. On the other hand, model matches to the observed spectra point to a lower reddening ($\mathrm{E}(B-V) \sim 0.30$). In some respects, SN 2002bo behaves as a typical "Branch normal" type Ia supernova (SN Ia) at optical and IR wavelengths. We find a B-band risetime of 17.9±0.5 days, a Δm_{15}(B) of 1.13 ± 0.05, and a de-reddened $M_B = -19.41 \pm 0.42$. However, comparison with other type Ia supernovae having similar Δm_{15}(B) values indicates that in other respects SN 2002bo is unusual. While the optical spectra of SN 2002bo are very similar to those of SN 1984A (Δm_{15}(B) = 1.19), lower velocities and a generally more structured appearance are found in SNe 1990N, 1994D and 1998bu. For supernovae having Δm_{15}(B) > 1.2, we confirm the variation of $\mathcal{R}$(SiII) (Nugent et al. 1995) with Δm_{15}(B). However, for supernovae such as SN 2002bo, with lower values of Δm_{15}(B) the relation breaks down. Moreover, the evolution of $\mathcal{R}$(SiII) for SN 2002bo is strikingly different from that shown by other type Ia supernovae. The velocities of SN 2002bo and 1984A derived from SII 5640Å, SiII 6355Å and CaII H&K lines are either much higher and/or evolve differently from those seen in other normal SNe Ia events. Thus, while SN 2002bo and SN 1984A appear to be highly similar, they exhibit behaviour which is distinctly different from other SNe Ia having similar Δm_{15}(B) values. We suggest that the unusually low temperature, the presence of high-velocity intermediate-mass elements and the low abundance of carbon at early times indicates that burning to Si penetrated to much higher layers than in more normal type Ia supernovae. This may be indicative of a delayed-detonation explosion.

Key words: Supernovae: general – Supernovae: 2002bo

1 INTRODUCTION

Thermonuclear (type Ia) supernovae (SNe Ia) are believed to originate from the thermonuclear disruption of

a white dwarf composed of carbon and oxygen. In the favoured scenario, the white dwarf accretes mass (mostly hydrogen) from a companion star in a binary. However, the identification of the progenitor type is by no means certain. Alternative initial scenarios include the merging of two binary white dwarfs, or the accretion of helium (Hillebrandt & Niemeyer 2000). It is generally accepted that when the degenerate mass reaches the Chandrasekhar limit (1.4 $M_{\odot}$), explosive carbon ignition occurs and burning to nuclear statistical equilibrium ensues, forming mostly radioactive ^{56}Ni. Intermediate-mass nuclei, e.g. ^{28}Si, are produced in the outer, lower-density regions. These elements give rise to the typical observed spectra of SNe Ia, which are dominated by lines of Fe, Si and S. Nevertheless, the details of the explosion mechanism are still poorly understood. For example, it is not clear whether nuclear burning proceeds entirely in the form of a deflagration, or whether a subsequent transition to a detonation wave occurs. Also, we do not understand fully what determines the mass of ^{56}Ni produced, or if events producing the same ^{56}Ni mass can differ in other respects.

It is vital that we improve our understanding of SNe Ia both for the insight they can provide about astrophysical processes taking place under extreme conditions, and because of their use in the measurement of cosmological distances. Observational studies of SNe Ia at high redshifts ($z \sim 0.3 - 1.2$) are yielding increasingly strong evidence that we are living in a Universe whose expansion began to accelerate at half its present age. This finding is commonly taken to indicate a finite positive cosmological constant Λ (Riess et al. (1998); Perlmutter et al. (1999)) i.e. a new form of energy with negative pressure (Caldwell et al. 1998). However, an important caveat is that these cosmological conclusions rely on the assumption that the physical properties of high–z SNe Ia are the same as those seen locally. But given the uncertainties in the nature of local SNe Ia, it is important to test the validity of this assumption. In order to address this fundamental question we must endeavour to improve our physical understanding of the SN Ia phenomenon.

SN Ia theoretical models must be tested and constrained through comparison with observed light curves and spectral evolution. Yet only for a few events has even moderate coverage been achieved, especially at infrared wavelengths. Moreover, at all wavelengths there is a scarcity of observations during the 2–3 weeks when the SN is still brightening. Data obtained during this time can be particularly effective in setting tight model constraints (Riess et al. 1999). A minority of SNe Ia are obviously peculiar (Leibundgut et al. (1993); Turatto et al. (1996); Turatto et al. (1998); Li et al. (2001)), although their significance for the overall picture is not clear. However, even the so-called "normal" SNe Ia display differences from one to another, e.g. in the photospheric expansion velocities deduced from the lines of the intermediate mass elements (IME) (Branch et al. (1988); Barbon et al. (1990)). Other more subtle differences in the photospheric spectra can also be seen.

The desire to make decisive progress in accounting for the observed behaviour and diversity of SNe Ia in terms of the explosion physics and the nature and evolution of the progenitor provided the motivation for the recently formed European Supernova Collaboration (ESC). This comprises a large consortium of European groups specialising in the observation and modelling of SNe Ia. The consortium is partially funded as an EU Research Training Network. The ESC aims to elucidate the nature of SNe Ia through the acquisition of high-quality photometry and spectra for 10–12 nearby SNe Ia. These data will be used to constrain state-of-the-art models for the explosion and progenitor, also under development by the ESC.

Our first target, SN 2002bo in NGC 3190 (SA-LINER type), was discovered independently by Cacella and Hirose (Cacella et al. 2002) in CCD images taken on Mar. 9.08 UT and Mar. 9.505, respectively. It lies at the edge of a dust lane. Soon after discovery, SN 2002bo was classified as a type Ia SN at an early epoch, with the discovery date being about 2 weeks before maximum light (Kawakita et al. (2002), Benetti et al. (2002), Matheson et al. (2002) and Chornock et al. (2002)). The high expansion velocity (about 17,700 $\mathrm{km\,s^{-1}}$) of the Si II 6355Å doublet was particularly indicative of an early epoch. In this paper we describe the results of our photometric and spectroscopic monitoring campaign for SN 2002bo, and compare the observed properties with those of a sample of Branch-normal (Branch et al. 1993) SNe Ia. We also modelled two of the optical spectra, the earliest one and one very close to maximum, in order to derive some of the properties of the SN ejecta. We address the problem of determining the epoch of the spectra and in particular the reddening to the SN. We have also modelled our earliest IR spectrum both to address the amount of primordial carbon left in the SN ejecta and to identify the transitions present in this spectrum.

2 OBSERVATIONS

Spectroscopy and imaging were carried out at several sites using a number of different telescopes and/or instruments (Tables 2 & 5).

2.1 Optical Photometry

The CCD frames were first debiased and flat-fielded in the usual manner. Since most of the data were obtained under non-photometric conditions, relative photometry was derived with respect to a local sequence of field stars (see Fig. 1). The three photometric nights marked in table 2 (plus one VLT+FORS1 observation of SN 2002bo on March 3rd, 2003) were used to calibrate this sequence against Landolt standard stars (Landolt 1992). The magnitudes and estimated errors of the local standards are shown in Table 1. These magnitudes were obtained by summing the counts through an aperture, the size of which varied according to the seeing. The telescope+instruments used for covering the SN 2002bo light curves appear to define a reasonably homogeneous photometric system. No systematic deviations are apparent in any photometric band (Fig. 2). This holds even for the S70 and INT photometric systems which have high colour terms

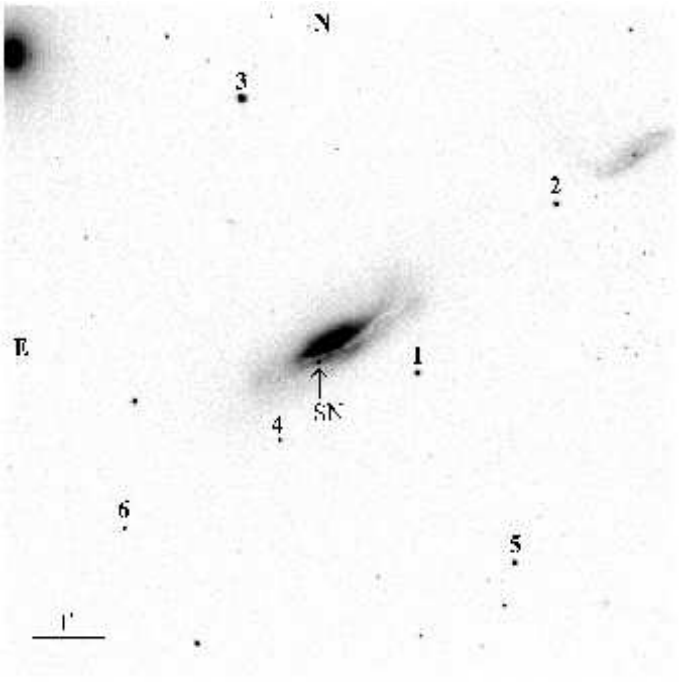

Figure 1. SN 2002bo in NGC 3190 and reference stars. The image is in the I band and was taken with the TNG+DOLORES on 2002 May 6.

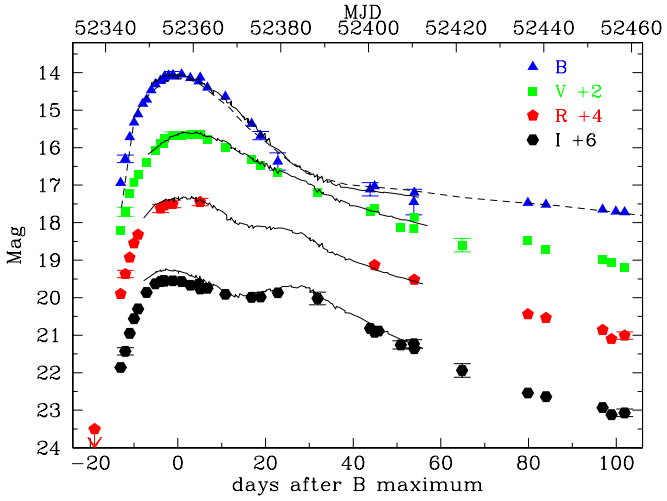

Figure 2. B,V,R and I light curves of SN 2002bo. The R limit of Sarneczky & Bebesi 2002 is also shown. The solid lines represent the B,V,R and I light curves of SN 1998bu (Suntzeff et al. 1999, Jha et al. 1999, Hernandez et al. 2000) adjusted to the SN 2002bo distance and reddening (see Sect. 2.3). A distance modulus of 30.25 (Tanvir et al. 1999) and a reddening of 0.33 (Phillips et al. 1999) have been assumed for SN 1998bu. The dashed line is the B light curve of SN 1984A (Barbon, Rosino & Iijima, 1989). In this case the light curve has been arbitrarily shifted in magnitude to fit the SN 2002bo B maximum.

Table 1. Magnitudes of local sequence stars identified in Fig. 1

star	B	V	R	I
1	15.19 ± 0.02	14.39 ± 0.04	13.96 ± 0.05	13.58 ± 0.02
2	15.01 ± 0.03	14.28 ± 0.06	13.84 ± 0.05	13.52 ± 0.02
3	13.03 ± 0.09	12.37 ± 0.08	11.98 ± 0.08	11.64 ± 0.08
4	18.47 ± 0.04	17.18 ± 0.03	16.31 ± 0.04	15.63 ± 0.04
5	16.31 ± 0.04	15.65 ± 0.06	15.24 ± 0.07	
6	18.55 ± 0.06	17.90 ± 0.04	17.51 ± 0.08	17.16 ± 0.04

in the colour equations (S70 - I:$-0.40 \times (R-I)$; INT - B:$+0.23\times(B-V)$, V:$+0.135\times(B-V)$ and R:$+0.20\times(R-I)$).

Ideally, one would like to remove the galaxy background by subtraction of a galaxy "template" where the SN is absent. This procedure was indeed applied to some of the S70 observations, especially those with complex background (mostly I frames) around the SN. However, for most of the data a suitable template image was not available. Therefore, in such cases the SN magnitudes were measured using the IRAF point-spread-function fitting task Daophot. This procedure allows the simultaneous fitting and subtraction of the galaxy background. While the pixel scales varied from one instrument to another, they were always sufficiently small to provide good sampling of the PSFs (see Table 2 caption). For cases in which the seeing is fair, the SN is relatively bright, and its PSF well-sampled, it has been found that this method produces results in excellent agreement with the template subtraction method (cf. Rigon et al. (2000)). Our results confirm this. The supernova magnitudes are presented in Tab. 2. The table lists the date (col.1), Modified Julian Day (col.2), epoch relative to $t_{B_{max}}$ (col.3), BVRI magnitudes with estimated internal errors in parentheses (cols.4–7), the telescope used (col.8), and the seeing for each epoch, averaged over the observed bands (col.9).

2.1.1 *Light curves and rise times*

The B, V, R and I light curves of SN 2002bo are shown in Fig. 2, including the pre-discovery limit of Sarneczky & Bebesi (2002). The light curves are very well sampled, spanning epochs from just a few days after the explosion to 100 days post-maximum. We used a high order Legendre polynomial to fit the points around maximum, and hence infer a $B_{max} = 14.04 \pm 0.10$ mag on $t_{B_{max}}$=MJD 52356.0 ± 0.5 (2002 March 23.0 UT). Thus, our observations cover epochs between –13 and +102 days with respect to $t_{B_{max}}$. Likewise, we found $V_{max} = 13.58 \pm 0.1$ mag, and occurring about two days after $t_{B_{max}}$, in agreement with the template light curves derived by Leibundgut (1991a). The corresponding values for the other two bands are $R = 13.49 \pm 0.10$ and $I = 13.52 \pm 0.10$ and occurred respectively about 1 day after and about 2.4 days before $t_{B_{max}}$. The tendency for the I-band peak to occur before $t_{B_{max}}$ has been observed in other SNe Ia e.g. SN 1998bu (Hernandez et al. 2000). The secondary I maximum has been reached on $= MJD$ 52381.5 (e.g. $\sim$ 30d after and 0.35mag below the primary maximum). From the B light curve we derive a post-maximum decline of Δm_{15}(B)$= 1.13 \pm 0.05$.

Thanks to the early detection and good temporal coverage of SN 2002bo we have been able to estimate the risetime to maximum and hence the explosion epoch t_0, following Riess et al. (1999). The main hypothesis of this method is

Table 2. Photometric measurements for SN 2002bo

date	M.J.D.	epoch* (days)	B	V	R	I	tel.	avg seeing (arcsec)
9/3/02	52342.95	–13.1	16.94 (0.04)	16.22 (0.03)	15.90 (0.03)	15.86 (0.03)	A1.82	2.4
11/3/02	52344.01	–12.0	16.30 (0.10)	15.71 (0.12)	15.37 (0.10)	15.43 (0.10)	A1.82	1.5
12/3/02	52345.02	–11.0	15.72 (0.06)	15.22 (0.03)	14.93 (0.05)	14.95 (0.06)	A1.82	2.3
12/3/02	52345.99	–10.0	15.33 (0.07)	14.93 (0.07)	14.55 (0.05)	14.56 (0.06)	A1.82	2.2
13/3/02	52346.92	–9.1	15.11 (0.03)	14.71 (0.03)	14.32 (0.03)	14.30 (0.03)	A1.82	2.6
15/3/02	52348.02	–8.0	14.83 (0.03)				NOT	1.1
15/3/02	52348.89	–7.1	14.72 (0.03)	14.39 (0.02)		13.86 (0.04)	S70	2.6
16/3/02	52349.92	–6.1	14.47 (0.04)				NOT	0.9
17/3/02	52350.89	–5.1	14.31 (0.06)	14.07 (0.02)		13.63 (0.05)	S70	2.0
19/3/02	52352.04	–4.0	14.22 (0.03)				NOT	3.2
19/3/02	52352.05	–4.0	14.22 (0.05)	13.88 (0.07)	13.62 (0.11)	13.57 (0.08)	A1.82	3.0
19/3/02	52352.75	–3.3	14.17 (0.03)	13.88 (0.02)		13.54 (0.03)	S70	1.4
19/3/02	52352.96	–3.0	14.10 (0.04)	13.76 (0.03)	13.54 (0.05)	13.56 (0.04)	A1.82	3.7
20/3/02	52353.89	–2.1	14.08 (0.02)				NOT	3.1
21/3/02	52354.84	–1.2	14.07 (0.10)	13.68 (0.10)	13.50 (0.10)	13.55 (0.10)	A1.82	2.0
21/3/02	52354.95	–1.1	14.08 (0.07)				NOT	1.1
23/3/02	52356.87	0.9	14.05 (0.05)	13.68 (0.02)		13.57 (0.02)	S70	1.8
25/3/02	52358.85	2.9	14.14 (0.06)	13.64 (0.03)		13.67 (0.04)	S70	1.7
27/3/02	52360.74	4.7	14.23 (0.04)	13.65 (0.02)		13.64 (0.03)	S70	1.5
28/3/02	52361.08	5.1	14.13 (0.06)	13.66 (0.04)	13.45 (0.10)	13.77 (0.04)	JKT	2.0
29/3/02	52362.74	6.7	14.40 (0.04)	13.77 (0.02)		13.75 (0.02)	S70	1.9
2/4/02	52366.84	10.8	14.64 (0.04)	14.00 (0.02)		13.91 (0.05)	S70	3.4
8/4/02	52372.85	16.9	15.36 (0.06)	14.31 (0.02)		13.99 (0.05)	S70	1.5
10/4/02	52374.89	18.9	15.68 (0.11)	14.47 (0.03)		13.98 (0.05)	S70	1.7
14/4/02	52378.8	22.8	16.37 (0.23)	14.66 (0.03)		13.87 (0.03)	S70	1.4
23/4/02	52387.88	31.9		15.20 (0.03)		14.02 (0.17)	S70	1.5
5/5/02	52399.86	43.9	17.11 (0.18)	15.70 (0.05)		14.82 (0.06)	S70	1.6
6/5/02**†	52400.89	44.9	17.03 (0.05)	15.63 (0.05)	15.13 (0.05)	14.92 (0.05)	TNG	1.9
7/5/02	52401.82	45.8				14.89 (0.07)	S70	6.5
12/5/02	52406.85	50.9		16.13 (0.05)		15.26 (0.11)	S70	2.6
15/5/02	52409.83	53.8	17.45 (0.34)	16.16 (0.06)		15.23 (0.11)	S70	1.7
15/5/02	52409.95	54.0	17.20 (0.08)	15.86 (0.06)	15.52 (0.03)	15.36 (0.04)	A1.82	2.1
26/5/02	52420.86	64.9		16.60 (0.18)		15.94 (0.18)	S70	4.0
10/6/02	52435.87	79.9	17.47 (0.07)	16.47 (0.06)	16.44 (0.08)	16.54 (0.04)	A1.82	2.6
14/6/02	52439.98	84.0	17.52 (0.07)	16.71 (0.06)	16.54 (0.04)	16.64 (0.05)	NTT	0.7
27/6/02	52452.92	96.9	17.65 (0.04)	16.98 (0.04)	16.86 (0.04)	16.93 (0.09)	INT	1.1
29/6/02†	52454.94	98.9		17.06 (0.06)	17.10 (0.04)	17.12 (0.06)	JKT	1.4
30/6/02	52455.92	99.9	17.70 (0.05)				JKT	2.0
2/7/02†	52457.94	101.9	17.72 (0.08)	17.20 (0.05)	17.01 (0.10)	17.07 (0.10)	JKT	2.6

∗ Epoch relative to B_{max}, which occurred on MJD=52356.0 = 2002 March 23.0 UT
∗∗ We also have a U-band measurement at this epoch of $U = 17.58 \pm 0.05$
† Photometric night
A1.82 = Asiago1.82m telescope + AFOSC; pixel scale=0.473"/px
NOT = Nordic Optical Telescope + ALFOSC; pixel scale=0.188"/px
S70 = 0.70m Sternberg Astronomical Institute telescope + CCD Camera; pixel scale=1.00"/px
JKT = 1.0m Jacobus Kapteyn Telescope + CCD camera; pixel scale=0.330"/px
TNG = Telescopio Nazionale Galileo + DOLORES; pixel scale=0.275"/px
NTT = ESO NTT + EMMI; pixel scale=0.1665"/px
INT = 2.5m Isaac Newton Telescope + WFC; pixel scale=0.333"/px

that the early luminosity (for epochs $t_0 \lesssim 10$ days) is proportional to the square of the time since explosion. We find $t_0(B)$ =MJD 52338.7 ± 0.6, $t_0(V)$ =MJD 52338.1 ± 0.8, $t_0(R)$ =MJD 52339.2 ± 0.8 and $t_0(I)$ =MJD 52338.3 ± 1.0. Thus there is reasonable agreement between the bands as to the explosion epoch, viz. MJD= 52338.1 ± 0.5. The B-band risetime of 17.9±0.5 days is consistent with the Riess et al. value of 18.7 ± 0.6 days for a SN Ia with the $\Delta m_{15}(B)$ of SN 2002bo. However, our explosion epoch is in better agreement with the −17.6 ± 0.05 days for SN 1994D derived by Vacca & Leibundgut (1996) through empirical light curve fitting of B, V and R photometry. Finally, we note that the explosion epoch derived from modelling of the SN 2002bo spectra (see Sect. 2.5) is −18 ± 1 days, which is consistent with our photometry-based value.

2.1.2 Colour evolution

In Fig. 3 we show the intrinsic $B-V$, $V-R$ and $V-I$ colours and their evolution. The $B-V$ colour was dereddened by 0.43 mag, with corresponding values being applied to the other two colours (see subsection 2.2). The

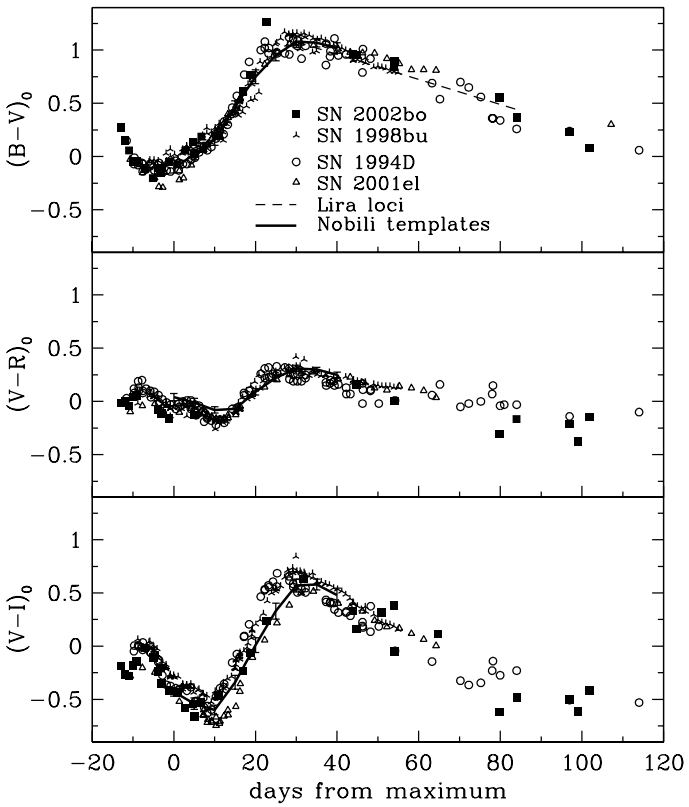

Figure 3. De-reddened $B-V$, $V-R$ and $V-I$ colour evolution of SN 2002bo compared with that of SN 1994D (Patat et al 1996), SN1998bu (Suntzeff et al. 1999, Jha et al. 1999, Hernandez et al. 2000), 2001el (Krisciunas et al. 2002) and the Nobili colour-curve templates (Nobili et al. 2003). In the upper panel, the dashed line shows the Lira loci which describes the later $B-V$ colour evolution of unreddened SNIa.

law of Cardelli et al. (1989) was used for de-reddening. Also shown is the colour evolution of SNe 1994D, 1998bu and 2001el, together with the colour templates (with their intrinsic dispersions) of Nobili et al. (2003) for $0-40$ days, and the loci of Lira (Lira (1995), Phillips et al. (1999)). The 3 comparison SNe have $\Delta m_{15}(B)$ values of, respectively, 1.32, 1.01 and 1.13. Similarly to SN 1994D, two weeks before maximum the intrinsic $B-V$ colour is quite red, viz. $(B-V)_0 \sim +0.28$, but it moves rapidly blueward reaching a minimum of -0.12 around -4^d. SNe 1994D, 1998bu and 2001el display a similar behaviour, although SN 2001el shows a slightly deeper minimum. The curve then moves redward such that by day +23 it appears to reach a maximum at $(B-V)_0 \sim 1.27$, about 0.2 mag redder than for the comparison SNe. The curve then follows a typical evolution to the blue, reaching a value close to zero by $+100^d$. The Nobili et al. template nicely describes the $B-V$ evolution in the $0-40$ day era.

The $V-R$ colour curve of SN 2002bo exhibits a behaviour which is very similar to those of the comparison SNe. Only near maximum does the SN 2002bo curve depart from the general trend, showing values which are about 0.10 mag. bluer. The Nobili template fails to describe the $V-R$ evolution of our SN Ia sample especially around phase +10days. The $V-I$ colour evolution of SN 2002bo is very similar both to those of the comparison SNe, and to the Nobili template.

2.2 Near-infrared Photometry

Near-infrared imaging (JHK) was carried out at four epochs around maximum light at the 1.55m Carlos Sánchez Telescope (TCS), Tenerife using the CAIN infrared camera. This uses a 256 x 256 HgCdTe array and was operated at a plate scale of 1.0 arcsec/pixel. In addition a single epoch observation at JHKs was obtained about 2 weeks after maximum light using at the 2.5m Nordic Optical Telescope (NOT) and the NOTCam infrared camera. This uses a 1024x1024 HgCdTe detector with a plate scale of 0.23 arcsec/pixel. Data reduction was carried out using standard routines within IRAF. The individual co-add frames ($\sim 10-50$ per pointing) taken with TCS have been aligned before to be combined. This was necessary because of the inaccuracy of the telescope tracking. Simple aperture photometry of the TCS images was carried out using the Starlink package Gaia (Starlink User Note 214, 2003, P.W. Draper, N.Gray & D.S. Berry). An aperture radius of 2 arcseconds was chosen. This was a compromise between including as much target signal and excluding as much galaxy background as possible. The sky annulus had inner and outer radii of 3.4 and 5.0 arcsec respectively. However, the relatively large plate scale of the CAIN camera together with the presence of a strong galaxy background meant that the magnitude uncertainties, especially in the H and K bands, are large (∼0.1 to 0.2 mags). Before photometric measurement of the NOTCam data was carried out, a smoothed background was subtracted from the area of the supernova. This, together with the finer plate scale of NOTCam, yielded magnitudes of higher precision. Therefore, in order to preserve as much information as possible about the IR evolution of the supernova, the TCS magnitudes were calibrated using the NOTCam images via two field stars lying, respectively, about (81"W, 7"S) and (32"E, 61"S) of the supernova. This also meant that the earliest TCS epoch could be used in spite of there being no standards available for that night. For the NOTCam calibration, use was made of photometric standards listed in Hunt et al. (1998) and Persson et al. (1998). The resulting magnitudes are given in Table 3

Within the uncertainties, the photometry shows that the IR magnitudes of SN 2002bo evolved in a manner typical of Type Ia supernovae. In the J-band, where the precision is higher, we can deduce that maximum light in this band was about 3 days before maximum light in B. Similar behaviour has been seen in other SNe Ia (e.g. SN 1998bu: Hernandez et al. (2000)). In addition the rapid fading in the J-band by +14 days is also typical. We note that a more extensive, high precision study of the SN 2002bo IR photometric evolution has been carried

Table 3. Near-infrared photometry of SN 2002bo

date	M.J.D.	epoch* (days)	J	H	K	tel.
18/3/03	52351.5	-4.5	13.83(0.08)	13.96(0.13)	13.70(0.17)	TCS
20/3/03	52353.6	-2.4	13.70(0.09)	13.87(0.21)	13.61(0.15)	TCS
22/3/03	52355.5	-0.5	13.88(0.08)	13.75(0.20)	13.70(0.21)	TCS
24/3/03	52357.5	1.5	14.01(0.09)	13.95(0.16)	13.56(0.11)	TCS
5/4/03	52370.4	14.4	15.50(0.07)	14.23(0.02)	14.12(0.05)(Ks)	NOT

$*$ Epoch relative to B_{max}, which occurred on MJD=52356.0 = 2002 March 23.0 UT
TCS = Carlos Sánchez Telescope + CAIN; pixel scale = 1.0"/px
NOT = Nordic Optical Telescope + NOTCam; pixel scale = 0.23"/px

out by N. Suntzeff and K. Krisciunas at CTIO (private communication). To within the uncertainties, the two sets of data are consistent.

2.3 Reddening, distance and bolometric light curve

Lira (1995) and Phillips et al. (1999) found a uniform colour evolution in the $B-V$ colour of unreddened Type Ia SNe between +30 and +90 days. By de-reddening the observed SN 2002bo $B-V$ colour curve until it matched the Lira relation (Fig. 3), we deduced a colour excess of $\mathrm{E}(B-V) \sim 0.47$ mag. Only a minor fraction of this is due to extinction in the Galaxy ($\mathrm{E}(B-V)_{Gal} = 0.027$, Schlegel et al. (1998)), with the remaining $\sim$0.44 mag. being due to extinction in the host galaxy. That the light from SN 2002bo suffered significant extinction in the host galaxy is confirmed by strong NaID interstellar absorption lines at the redshift of NGC 3190. These lines have a total equivalent width $EW = 2.27 \pm 0.20$Å. Using the relation $\mathrm{E}(B-V) \gtrsim 0.16 \times EW(\mathrm{NaID})$ of Turatto et al. (2003) yields $\mathrm{E}(B-V)_{host} \gtrsim 0.36$, in good agreement with the value of 0.44 derived from the late photometry. Given the intrinsic dispersion in both the $\mathrm{E}(B-V) - EW(\mathrm{NaID})$ relation and the Lira relation, we conservatively adopt $\mathrm{E}(B-V) = 0.43 \pm 0.10$. We note, however, that spectral modelling (see Sect. 2.5) points to a lower reddening value of $\mathrm{E}(B-V) \sim 0.3$.

Adopting a redshift of +1405 $\mathrm{km\,s^{-1}}$and correcting for LG infall (+208 $\mathrm{km\,s^{-1}}$) onto the Virgo cluster (LEDA) with an adopted Virgo distance of 15.3 Mpc (Freedman et al. 2001) we derive a distance modulus of $\mu_B = 31.67$ (21.6 Mpc) for NGC 3190.

This value is adopted throughout the paper. Given the apparent peak magnitudes and the reddening, we obtain absolute peak intrinsic (i.e. de-reddened) magnitudes of $M_B = -19.41 \pm 0.42$, $M_V = -19.42 \pm 0.33$, $M_R = -19.18 \pm 0.25$, and $M_I = -18.93 \pm 0.18$ for SN 2002bo. As before, the law of Cardelli et al. (1989) was used for de-reddening. Given the uncertainties involved, the SN 2002bo magnitudes are consistent with the mean values given by Gibson et al. (2000) and Saha et al. (2001) for SNe Ia with Cepheid-determined distances. The average Δm_{15}(B) of these calibrators is 1.15 ± 0.14 (Altavilla et al. 2003), similar to that of SN 2002bo.

Table 4. Main parameter values for SN 2002bo and its host galaxy

Parent galaxy	NGC 3190
Galaxy type	SA(s)a pec sp LINER †
RA (2000)	$10^h18^m06^s.51$
Dec (2000)	+21°49'41".7
Recession velocity [$\mathrm{km\,s^{-1}}$]	1405 ‡
Distance modulus ($\mathrm{H_0} = 65$)	31.67
$\mathrm{E}(B-V)$	0.43 ± 0.10
Offset from nucleus	11".6E 14".2S
Explosion epoch (MJD)	52338.1 ± 0.5 (Mar 05, 2002)
Date of B maximum (MJD)	52356.0 ± 0.5 (Mar 23, 2002)
Magnitude at max	$B = 14.04 \pm 0.10$, $V = 13.58 \pm 0.10$, $R = 13.49 \pm 0.10$, $I = 13.52 \pm 0.10$
Δm_{15}(B)	1.13 ± 0.05

† NED
‡ LEDA, corrected for LG infall (208 $\mathrm{km\,s^{-1}}$)

The host galaxy of SN 2002bo, NGC 3190, belongs to the LGC 194 (Leo III) galaxy group (Garcia 1993), which contains 16 members. The surface brightness fluctuation method of distance determination (Tonry et al. 2001) has been applied to two of these viz. NGC 3193 and NGC 3226, yielding values of 32.66 ± 0.18 and $\mu = 31.86 \pm 0.24$, respectively. Together with the distance modulus for NGC 3190 derived above, this suggests considerable depth ($\sim$16 Mpc) in LGC 194, and may even cast doubts upon the group membership of NGC 3193.

Integrating the fluxes in the BVRI bands, adding the IR contributions at various epochs as discussed in Sect. 2.4.3, and applying the Contardo et al. (2000) and Suntzeff (1996) corrections for the missing U and UV contributions, respectively, we derived the uvoir luminosity for SN 2002bo (see Fig. 4). For comparison the uvoir light curve of SN 1998bu is also plotted. The similarity of the two light curves is remarkable. SN 2002bo reached bolometric maximum on MJD=52356 with logL=43.19 [$\mathrm{erg\,s^{-1}}$]. The date of the maximum and the rise time (about 17.4 days, calculated with the method described in the previous section) closely match the maximum date and rise time found for the B band.

A summary of the main parameter values for SN 2002bo and its host galaxy are given in Tab. 4.

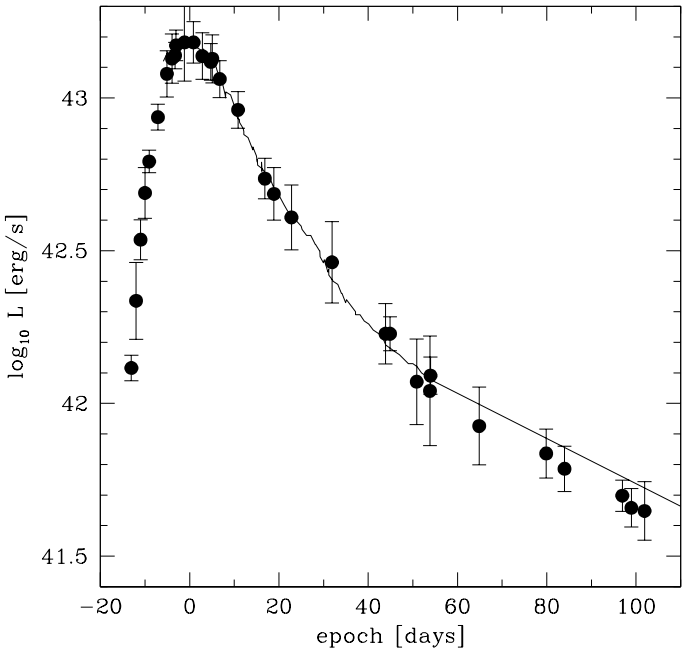

Figure 4. uvoir light curve of SN 2002bo. The solid line is the uvoir light curve of SN 1998bu reconstructed from the published UBVRI data and adding the UV and IR contributions given in Suntzeff (1996) for a sample of SNIa. The error bars refer only to the photometric errors and not to the uncertainty related to the reddening.

2.4 Spectroscopy

Spectroscopic observations spanned days –12.9 to +84, with exceptionally good temporal coverage being achieved during the risetime, allowing us to follow day-to-day variations. Table 5 lists the date (col.1), the Modified Julian Date (col. 2), the epoch relative to $t_{B_{max}}$ (col.3), the wavelength range (col.4), the instrument used (col.5), and the resolution as measured from the FWHM of the night-sky lines (col.6). On three epochs (∼–4, –2, –1 days), almost contemporary spectra were obtained at the A1.82 and NOT. These were co-added to produce the spectra shown for these epochs.

The spectra were reduced following standard FIGARO or IRAF routines. Extractions were usually weighted by the variance based on the data values and a Poisson/CCD model using the gain and read noise parameters. The background to either side of the SN signal was fitted with a low order polynomial and then subtracted. Fluxing was by means of spectrophotometric standard stars. The flux calibration of the optical spectra was checked against the photometry (using the IRAF task stsdas.hst_calib.synphot.calphot) and, where discrepancies occurred, the spectral fluxes were scaled to match the photometry. On nights with good observing conditions the agreement with photometry was within 10%. The flux calibration of the IR spectra was checked against JHK photometry. The fluxing was adjusted where necessary. The IR spectra on days +56/57/61 and day +85 were at later epochs than covered by the photometry. Therefore, the IR light curves of Meikle (2000) were used to extrapolate to these ephochs. The optical spectra are shown in Figure 5, and the IR spectra in Figure 12.

Table 5. Spectroscopic observations of SN 2002bo

Date	M.J.D.	epoch* (days)	range (Å)	tel.**	res. (Å)
10/03/02	52343.06	–12.9	3600-7700	A1.82	25
10/03/02	52343.99	–12.0	3600-7700	A1.82	25
11/03/02	52344.99	–11.0	3400-7700	A1.82	25
13/03/02	52346.91	–9.1	3400-7700	A1.82	25
14/03/02	52347.48	–8.5	8135-13060	UKIRT	25
14/03/02	52347.48	–8.5	14666-25400	UKIRT	100
15/03/02	52348.04	–8.0	3400-9050	NOT	14
16/03/02	52349.93	–6.1	3400-9050	NOT	14
18/03/02	52351.85	–4.1	3200-7550	WHT	2
19/03/02	52352.02	–4.0	3400-7700	A1.82	25
19/03/02	52352.05	–3.9	3400-9050	NOT	14
19/03/02	52352.94	–3.1	3400-7700	A1.82	25
20/03/02	52353.90	–2.1	3400-9050	NOT	22
20/03/02	52354.00	–2.0	3400-7700	A1.82	25
21/03/02	52354.88	–1.1	3400-7700	A1.82	25
21/03/02	52354.96	–1.0	3400-9050	NOT	22
22/03/03	52355.18	–0.8	3200-8900	WHT	12
23/03/02	52356.08	+0.1	3400-10350	A1.82	25
28/03/03	52361.94	+5.9	3100-8800	WHT	12
03/04/02	52367.29	+11.3	8180-13390	UKIRT	25
03/04/02	52367.29	+11.3	14725-25250	UKIRT	100
21/04/02	52385.40	+29.4	10680-13880	UKIRT	25
21/04/02	52385.40	+29.4	14780-25260	UKIRT	100
21/04/02	52385.91	+29.9	3500-9800	INT+I	4
23/04/02	52387.40	+31.4	8230-10980	UKIRT	25
01/05/02	52395.90	+39.9	3650-9200	INT+I	4
06/05/02	52400.94	+44.9	3250-8040	TNG	12
17/05/02	52411.90	+55.9	8155-10730	UKIRT	25
18/05/02	52413.00	+57.0	10730-13530	UKIRT	25
22/05/02	52417.00	+61.0	19840-25130	UKIRT	100
14/06/02	52440.00	+84.0	3900-9750	NTT	10
15/06/02	52440.99	+85.0	9400-16500	NTT+S	21

* - relative to the estimated epoch of B maximum (MJD=52356.0)
** - See note to Table 2 for telescope coding plus:
UKIRT = United Kingdom Infrared Telescope + CGS4
WHT = William Herschel Telescope + ISIS
INT+I = Isaac Newton Telescope + IDS
NTT+S = ESO NTT + SOFI

2.4.1 Optical spectra

Inspection of Figure 5 shows that the early blueward shift of the $(B-V)$ colour (Figure 3) is at least partly due to a gradual steepening of the continuum until about -4 days. Similarly, the subsequent reddening follows a gradual decrease in the continuum slope.

We compare the spectra of SN 2002bo with those of SNe 1984A, 1990N, 1994D and 1998bu at about 1 week pre-maximum in Fig. 6, and at maximum light in Fig. 7. All these SNe have a Δm_{15}(B) in the range 1.01–1.32, and so in this sense can be regarded as fairly typical. Nevertheless, spectral differences between the events are apparent. At ∼1 week pre-maximum (Fig. 6), starting at the shortest wavelengths we note that, unlike SNe 1990N

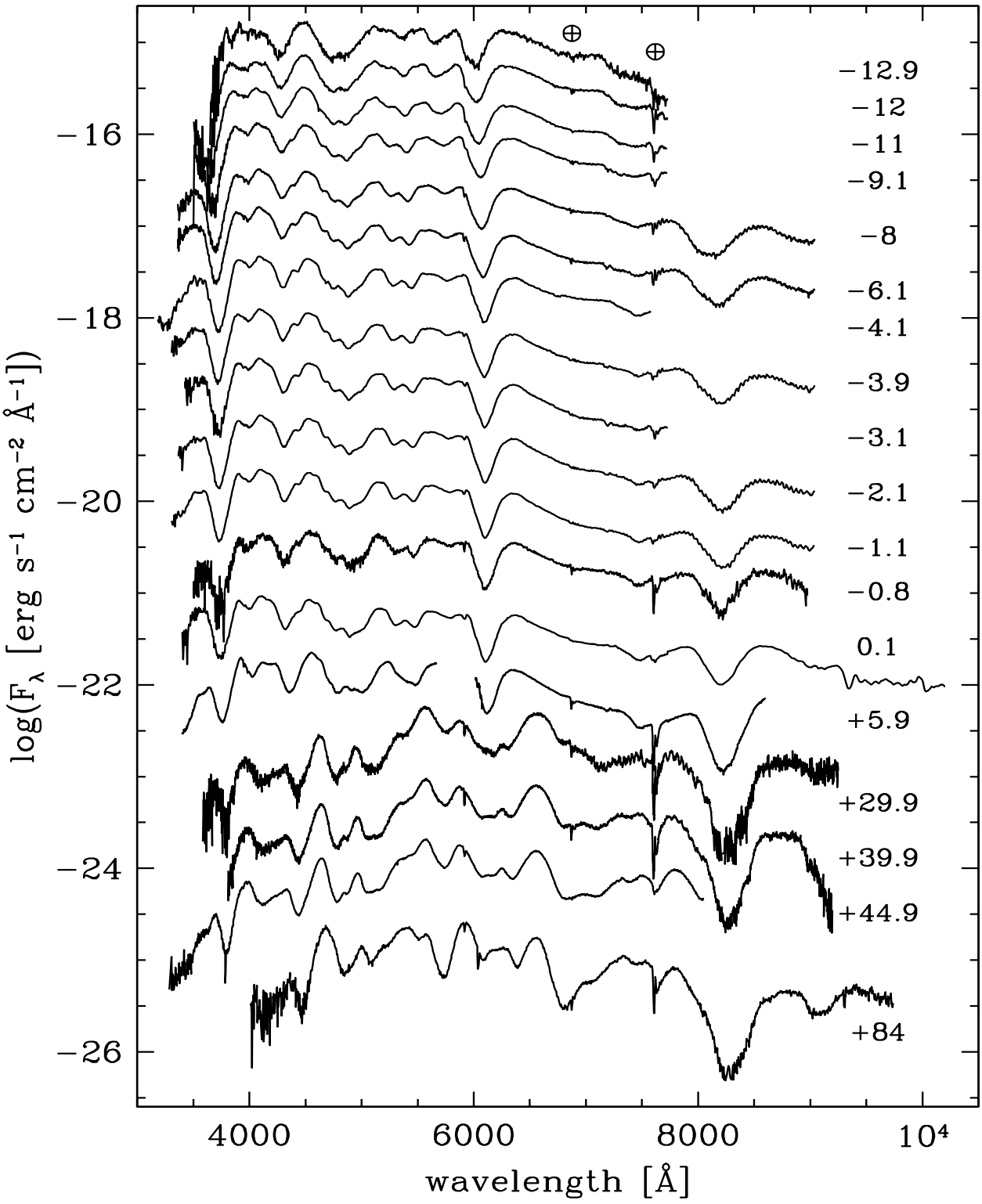

Figure 5. Spectral evolution of SN 2002bo. Wavelength is in the observer frame. The ordinate refers to the first spectrum, and the others have been shifted downwards by: 0.6, 1.2, 1.8, 2.4, 3, 3.6, 4.2, 4.8, 5.4, 6, 6.2, 7.4, 8, 8, 8.6, 9.2 and 9.2 respectively. Epochs are shown to the right of each spectrum. The ⊕ symbols show the main telluric features

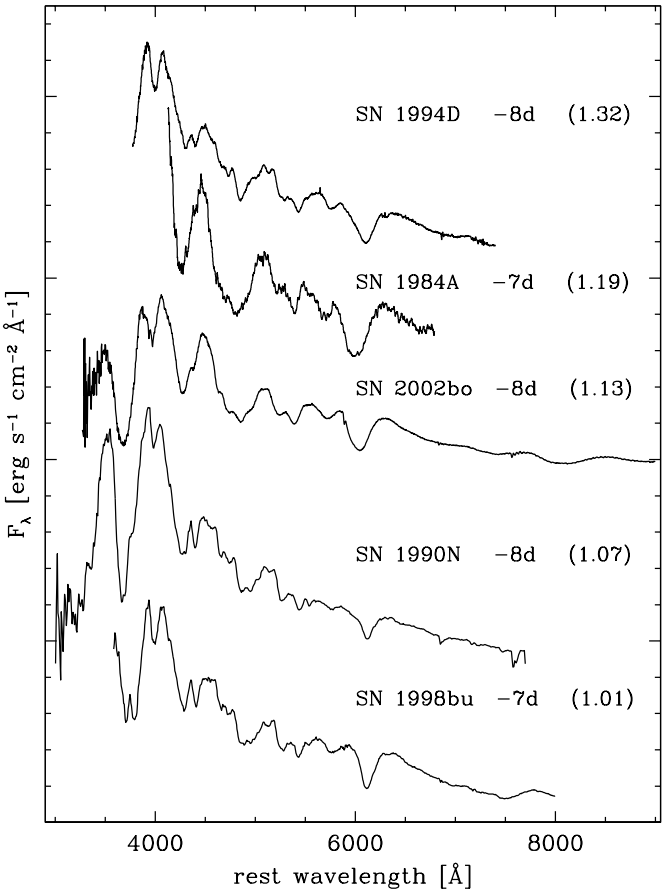

Figure 6. Comparison between spectra of SNe Ia about a week before maximum light arranged according to decreasing Δm_{15}(B) (given in parenthesis). The data sources are: SN 1998bu (Hernandez et al. 2000), SN 1994D (Patat et al. 1996), SN 1990N (Leibundgut et al. 1991b) and SN 1984A (Benetti, 1989). The spectra have been corrected for reddening and redshift. Epochs are shown to the right of each spectrum.

or 2002bo, SN 1998bu shows a double structure in the CaII H&K absorption feature. SN 1994D shows a similar double structure close to maximum light (Fig. 7), and this may well have also been present in its –8d spectrum. However, the spectral coverage stopped short of the this region. The prominent emission feature centered at about 4000Å varies somewhat between events owing to differing strengths in the SiII 4128, 4131Å doublet. The strength of this feature appears to be proportional to that of other SiII features in the various SNe. In the 4000-4500Å range, SN 2002bo and SN 1984A are rather similar in that they show a strong, absorption at ∼4250 Å, dominated by MgII 4481 Å, plus a weak absorption feature at ∼4400 Å due to SiIII 4553, 4568Å. In the other three SNe, the SiIII feature is much stronger, comparable in depth to the ∼4250 Å absorption which now contains both MgII 4481 Å as well as a significant contribution from FeIII (4419, 4433 Å etc.), as inferred from modelling and from the strength of the corresponding FeIII feature near 4950Å (FeIII 5074, 5127, 5156Å). Given the temperature sensitivity of the SiIII line, we can immediately conclude that both SNe 1984A and 2002bo have significantly cooler spectra than the other three SNe shown in Fig. 6. In the range 4500-5000Å, SNe 1984A and 2002bo show a strong and broad absorption (dominated by FeII lines including multiplet 48), showing little structure. In contrast, the other three SNe Ia show a much weaker absorption, but with a greater multiplicity of small features. Some of these differences may be due to higher velocities in SNe 1984A and 2002bo, leading to a greater degree of line blending. In the 5000–6000Å range, while the spectra of all five SNe Ia become more similar to one another, we nevertheless note a somewhat larger amount of structure in SNe 1990N, 1994D and 1998bu than in SNe 1984A and 2002bo. For example, a small dip at 5150Å is present only in the first three SNe. Longwards of 6000Å, we find that SNe 1984A and 2002bo show SiII 6355Å absorption profiles which are both broader and more intense than in the other three SNe Ia.

Turning our attention now to the maximum-light spectra SNe Ia (Fig. 7) we see that the differences between SNe 1984A and 2002bo on the one hand and SNe 1990N, 1994D and 1998bu on the other are similar to those seen at the earlier epochs. For example, the double structure in the CaII H&K absorption is still present in SN 1998bu and, as mentioned above, in SN 1994D (see also Hatano et al. (2000)). However, it remains absent in SN 2002bo. The 4000–5000Å region exhibits differences similar to those seen at earlier times, with a strong and relatively structureless emission feature at 4500Å dominating the SNe 1984A and 2002bo spectra, while the other three SNe Ia show much weaker but more structured features. Also, the SiII 6355Å absorption profiles continue to be broader and deeper in SNe 1984A and 2002bo.

Nugent et al. (1995) found that the ratio, $\mathcal{R}$(SiII), of the depth of the SiII 5972Å and SiII 6355Å absorption troughs near maximum light is related to the speed of decline (and therefore to the luminosity) of the event, and to the characteristic temperature of the spectrum. Slower, brighter decliners exhibit a smaller value of $\mathcal{R}$(SiII) at maximum. In Figure 8 we have plotted maximum-light $\mathcal{R}$(SiII) vs. Δm_{15}(B) for 11 SNe. These include our SNe Ia sample plus those presented in Nugent et al. (1995), and SN 1999ee (we found values of $\mathcal{R}$(SiII) for SNe 1990N and 1994D which are slightly different from those of Nugent et al. (1995): 0.21 and 0.33 vs. 0.16 and 0.29 respectively). Figure 8 shows that while the Nugent et al. relation holds for Δm_{15}(B)>1.2, at values smaller than this it breaks down.

We also investigated the variation with epoch of the Nugent et al. relation for SNe 1984A, 1990N, 1994D, 1998bu, 2002bo, 1999ee. Fig. 9 shows that as we move to pre-maximum epochs the value of $\mathcal{R}$(SiII) remains higher in the faster-declining SN 1994D (Δm_{15}(B)=1.32) than in the slower-declining SNe 1999ee, 1990N and 1998bu. SNe 1994D and 1998bu show low amplitude variations with epoch, without any strong trend, while SN 1990N and possibly SN 1999ee move to lower ratios at earlier epochs. However, SN 2002bo exhibits a strikingly different behaviour. $\mathcal{R}$(SiII) has a remarkably high value of 0.54 at an epoch of −13d, but then undergoes a dramatic decline, levelling out just a few days before maximum at $\mathcal{R}$(SiII)=0.17. This is the

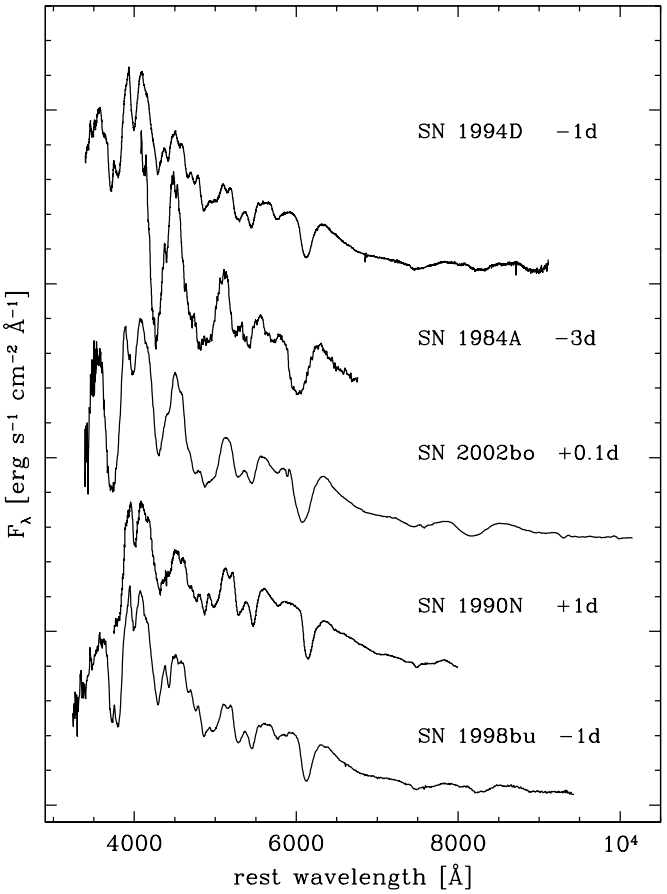

Figure 7. As for Fig. 6 but for spectra at maximum light.

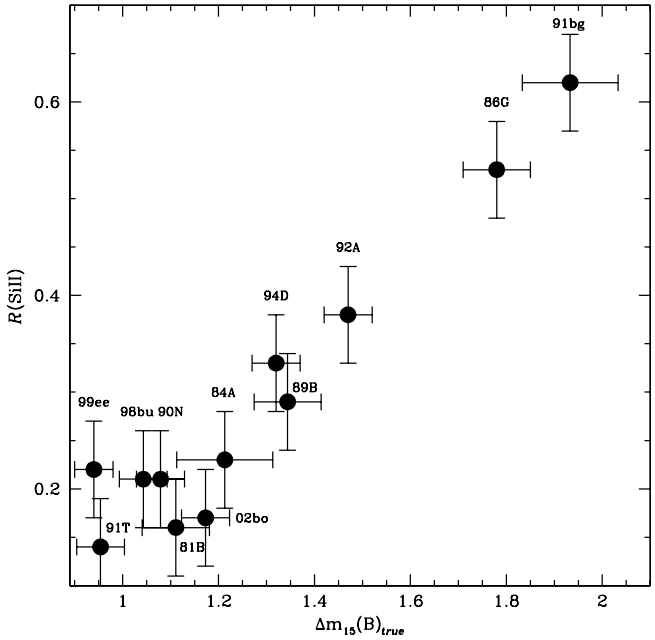

Figure 8. $\mathcal{R}$(SiII) vs. Δm_{15}(B) of the SNIa sample of Fig. 9 plus those presented in Nugent et al. 1995. Most of the Δm_{15}(B) have been taken from Phillips et al. (1999) but that of SN 1999ee (Stritzinger et al 2002), SNe 2002bo and 1984A (this paper). The Δm_{15}(B) have been corrected for the reddening effect (Phillips et al. 1999). The $\mathcal{R}$(SiII) of our sample have been measured by us the others have been taken from Nugent et al. (1995).

lowest value measured in the entire sample at this epoch. SN 1984A also seems to follow this trend, although it does not fall to such a low value. The decrease of $\mathcal{R}$(SiII) in SN 2002bo seems to track the increase of the photospheric temperature as indicated by the decrease of the $(B-V)$ colour (see Fig. 3) at these epochs.

2.4.2 The expansion velocities

Up to +5 days, SiII 6355Å provides one of the deepest absorption features. At the earliest epochs (see Figure 5), the profile is significantly asymmetric, owing in part to the presence of strong NaID interstellar absorption and the smaller equivalent width of the SiII feature at these early times. The minimum then shifts rapidly redwards and deepens with time as the photosphere moves into deeper, more slowly-moving material. This is illustrated in Fig. 10, which also shows the SiII 6355Å velocity evolution for SNe 1998bu, 1994D, 1990N, 1984A. The figure reveals clear differences between these events. SN 2002bo exibits an exceptionally high velocity which decreases in a smooth, gradual manner. A similar behaviour may be present in SN 1984A, although the data are more sparse. In contrast, SNe 1990N, 1994D and 1998bu show significantly lower velocities, with a distinct break in the decline rate around −5 days. The presence of a velocity break may be related to the fact that the velocity deduced from the SiII 6355Å absorption traces the photospheric velocity only during the era when the material near the photosphere is Si-rich. Later, the Si absorption region becomes more detached from the photosphere leading to a velocity which changes more slowly with time (Patat et al. 1996).

Lentz et al. (2000) computed emergent pre-maximum spectra for a grid of SNIa atmospheres and argued that some of the differences between SNe Ia events in the blueshift of the SiII 6355Å line at a given epoch may indicate a range of metallicities in the SNIa progenitor. In Fig. 10 we show the Lentz model velocity predictions for metallicity values of $\times 1/3$, $\times 3$ and $\times 10$ solar. While the behaviour of the lower velocity SNe Ia is plausibly encompassed by a metallicity range $\times 1/3$ to $\times 3$, a metallicity even as high as $\times 10$ solar fails to give velocities that are anywhere near those exhibited by SN 2002bo, not to mention the even faster SN 1984A. This suggests that the Si observed in these spectra is mostly the product of SN nucleosynthesis, and that the outer layers of the ejecta of SN 2002bo do not preserve much memory of the properties of the progenitor, as also indicated by the absence of the CII lines discussed below. Possible causes for this are discussed later.

We have also examined the evolution of the SII 5640Å absorption (Fig. 11a). This is an interesting line to study since, as it is quite weak, we can be reasonably certain that

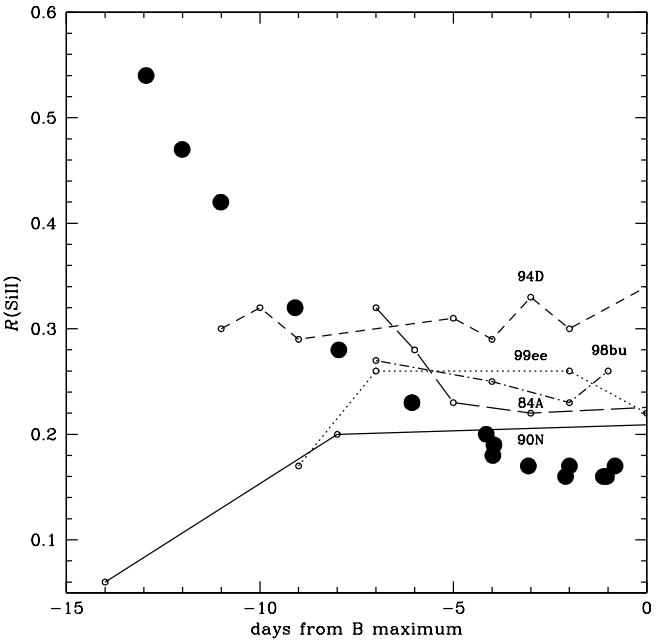

Figure 9. Evolution of $\mathcal{R}$(SiII) for a sample of SNe Ia. Solid circles refer to SN 2002bo data. The data sources are as in Fig. 6, SN 1999ee is from Hamuy et al. (2002). The Δm_{15}(B) values for SNe 1999ee, 1998bu, 1994D, 1990N and 1984A are 0.94 (Hamuy et al.), 1.01, 1.32, 1.07 (Phillips et al 1999) and 1.19 (this paper) respectively.

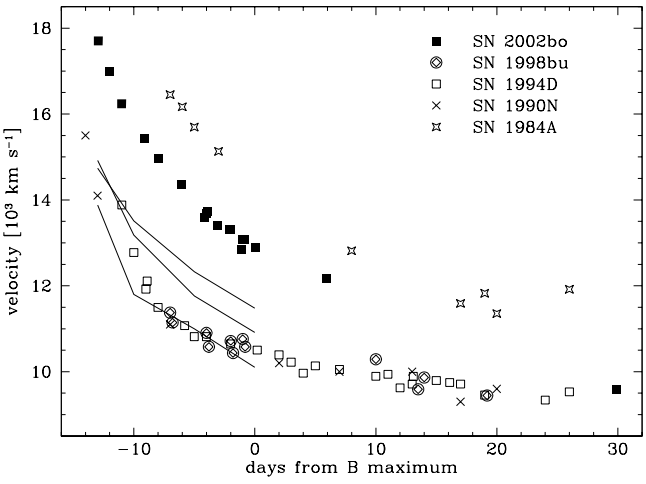

Figure 10. Evolution of the expansion velocity deduced from the minima of the SiII 6355Å absorption for SN 2002bo, SN 1998bu (Asiago archive, Hernandez et al. 2000), SN 1994D (Meikle et al. 1996, Patat et al. 1996), SN 1990N (Leibundgut et al. 1991b) and SN 1984A (Benetti, 1989). Also shown (solid lines) are the velocities predicted by the by Lentz et al (2000) model for cases of ×10 (top at epoch 0) , ×3 (middle) and ×1/3 (bottom) solar C+O layer metallicity

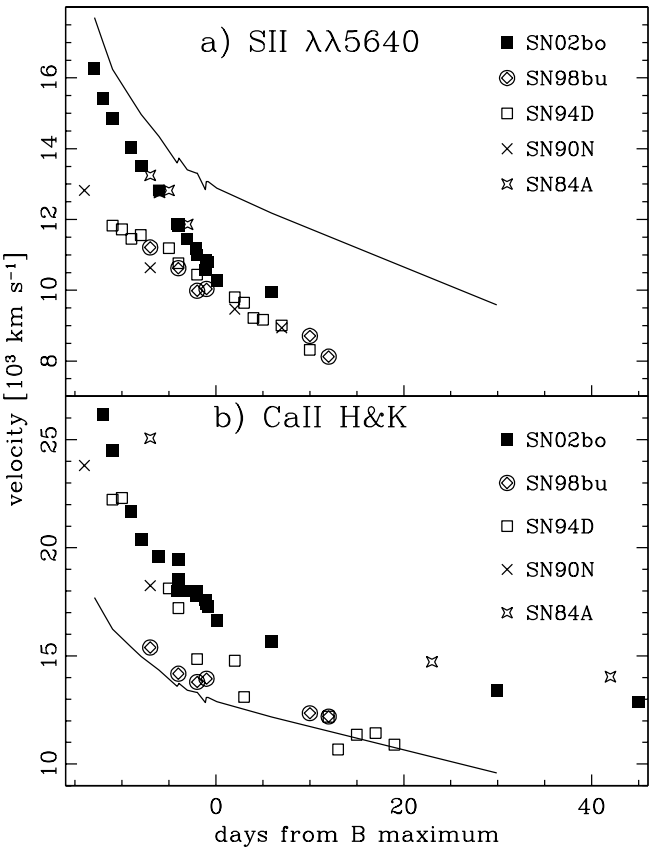

Figure 11. Evolution of the expansion velocities deduced from the minima of the SII 5640Å (a) and CaII H&K absorptions (b). The data sources are as in Fig. 10 apart from CaII H & K of SN 1984A which are from Wegner & McMahan (1987) and the McDonald Observatory (unpublished). For comparison, the SN 2002bo expansion velocity from SiII 6355Å is also shown (solid line) in both panels.

it is always formed close to the continuum photosphere (even allowing for possible SiIII 5740Å contamination at early times (Mazzali 2001)). Thus, it is a valuable probe of the true photospheric velocity. Curiously, the pre-maximum velocity behaviour appears to divide our sample into two groups. In SN 2002bo, the SII velocity declines from a value of over 16,000 km/s at –13 days to about 10,000 km/s at maximum. A similar behaviour is observed in SN 1984A, where the velocity is even slightly higher, although here the data do not begin until about –7 days. In contrast, the other SNe Ia reach only ∼12,500 km/s at –13 days, but they also decline to 10,000 km/s at maximum. This suggests rather different conditions in the outer envelopes of the two groups. Between 0 and +10 days, SNe 1990N, 1994D and 1998bu appear to show roughly the same decline rate in the velocity of the SII 5640Å line. Coverage of SNe 1984A and 2002bo is insufficient to reach definite conclusions about their decline rate in this period. Actually, at phase +8 days the SII doublet has already disappeared in the SN 1984A spectrum.

The other very prominent absorption at early times

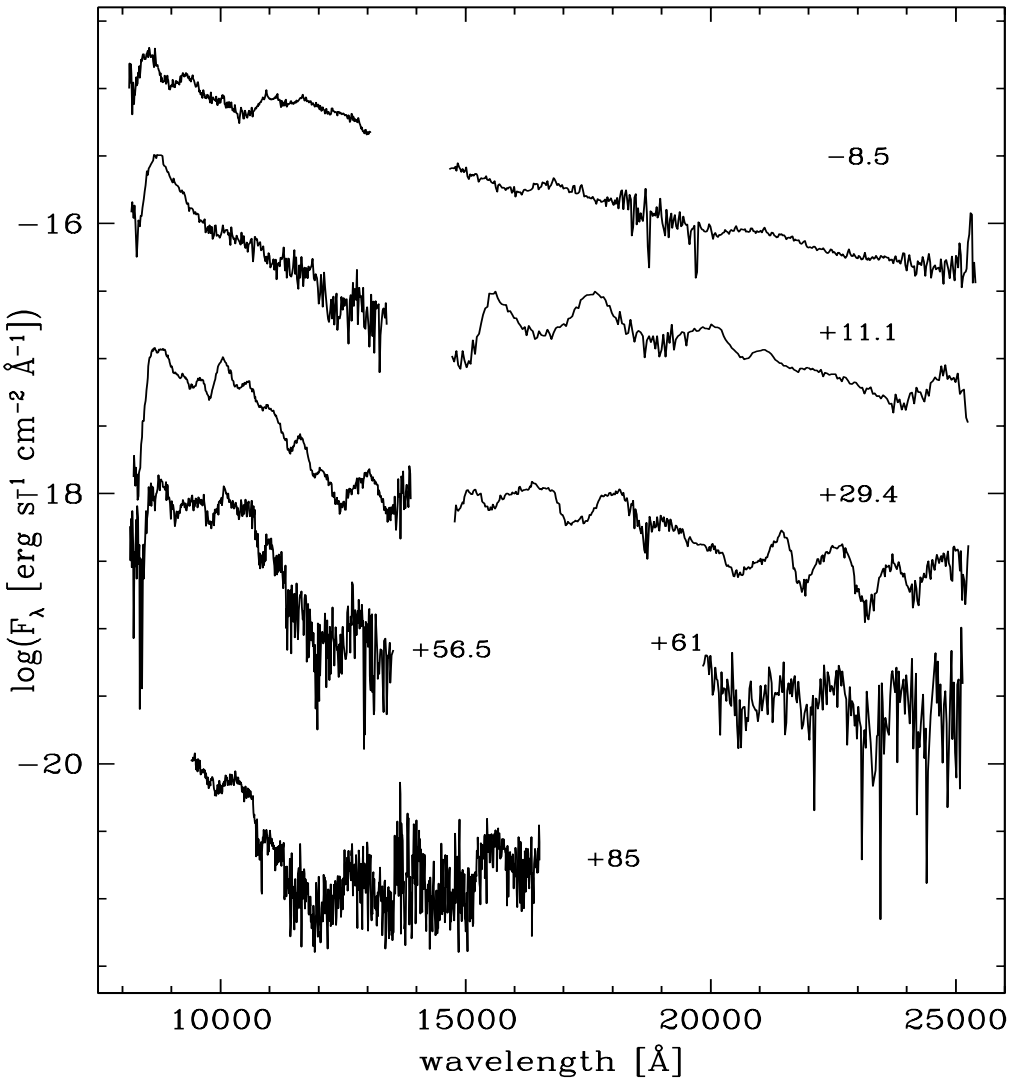

Figure 12. Spectral evolution of SN 2002bo in the infrared. Wavelength is in the observer frame. The ordinate refers to the first spectrum, and the others have been shifted downwards by: 1, 2.5, 2.9 and 4.4 respectively. Epochs are shown to the right of each spectrum.

is due to the CaII H&K doublet. At a given epoch this has an even higher optical depth than SiII 6355Å and so the line forms further out in the ejecta, in higher velocity layers. Consequently, the CaII H&K minima exhibit higher velocity blueshifts than those seen in contemporary SiII 6355Å minima (Fig. 11b). Up to maximum light, the CaII H&K velocities of SNe 1990N, 1994D, and SN 2002bo are similar, while SN 1998bu shows velocities which are slower by about 4000 km s^{-1}. On the other hand, the velocity in SN 1984A is about 5000 km s^{-1} higher. By +10 days, the SN 1994D velocity has declined to values similar to those of SN 1998bu. On the other hand, the SN 2002bo velocity declines more slowly, so that by +10 days its interpolated value exceeds those of SN 1994D and SN 1998bu by ∼3000 km s^{-1}. By about day +20, the SN 1984A velocity is only 1000 km s^{-1} faster than the interpolated value for SN 2002bo.

2.4.3 Infrared spectra

Inspection of Figure 12 shows the earliest IR spectrum (–8.5 days) to be largely featureless. A weak, complex P-Cygni line at about 10500 Å is apparent. This feature was first noted in the early spectra of SN 1994D (Meikle et al. 1996), who suggested either HeI 10830Å or MgII 10926Å as plausible identifications. More detailed modelling by Mazzali & Lucy (1998) yielded a similarly ambiguous identification. However, Wheeler et al. (1998) found that their models indicated that the feature should be due almost entirely to MgII. Our synthetic spectra (described below) tend to support the MgII identification. A broad, P-Cygni profile

(peak emission at ∼16700Å, rest frame) is also present, and Wheeler et al. (1998), Marion et al. (2003) attribute this to SiII 16910Å and MgII 16760/800Åwith the SiII dominant. Again, our synthetic spectra confirm this. At longer wavelengths the early IR spectrum is almost featureless except for a shallow, broad P-Cygni feature with a peak at ∼20800Å and attributed to SiII.

By +11 days, the spectrum has changed significantly, with a number of prominent emission features now being present. The 10500 Å feature has vanished (similar behaviour was seen in SN 1994D, (Meikle et al. 1996)), while two strong, wide (FWHM $\sim$ 11000km s^{-1}) emission features have appeared at 15490 Å and 17525Å. These are attributed to blends of CoII, FeII and NiII (Wheeler et al. (1998), Marion et al. (2003)). The deep, characteristic J-band deficit can also be seen (Spyromilio et al. 1994). This persists right through to the latest spectrum at +85 d. By one month post-maximum, three new broad emission peaks have appeared at 21350Å, 22490Å and 23619Å (rest frame), and these are attributed to Co, Ni and Si (Wheeler et al. 1998). They are still visible in the +56 day spectrum.

Hamuy et al. (2002) point out that the spectroscopic homogeneity among Branch-normal SNe Ia extends to the IR-domain. This is confirmed in Figure 13, where we compare the IR spectra of SNe 2002bo at −8.5d, +11.1d and +29.4d with those of SNe 1994D (Meikle et al. 1996)) and 1999ee Hamuy et al. (2002) at similar epochs. The main difference between the three SNe Ia is that the –8.5 d 10500Å feature is absent from the SN 1999ee spectrum. Since this feature is also clearly visible in SN 1999by (Hamuy et al. 2002) it seems that SN 1999ee is peculiar in this respect. We conclude that, as in the optical domain, there exists some inhomogeneity among the IR spectra of normal SNIa.

Figure 14 shows the overall optical+IR spectral evolution of SN 2002bo. This was created by combining IR and optical spectra having similar epochs. These collages have been used to determine the IR flux contribution for reconstructing the bolometric light curve (see Sect. 2.3). For the earliest spectrum, following de-reddening we find that the the total flux in the IR (integrated between 10000 and 25000 Å) is only 5% of the total optical flux (integrated between 3500 and 10000 Å). For the second one, taken near the secondary maximum of the IR light curves, the IR contribution rises to 18%. For the later two spectra the IR contribution decreases to 6% of the optical. This is in close agreement with the finding of Suntzeff (1996, 2003) who shows that more than 80% of the total SN Ia uvoir flux appears in the 3000-10000Å window.

2.5 Comparison of observed and synthetic spectra

In order to interpret more deeply our observations, we have computed synthetic spectra for some of the available epochs. These models not only provide us with information about the physical properties of the SN ejecta, such as temperature, chemical composition, etc., but also they can be used to verify observation-based estimates of parameters such as reddening, distance and epoch. We used a Monte Carlo

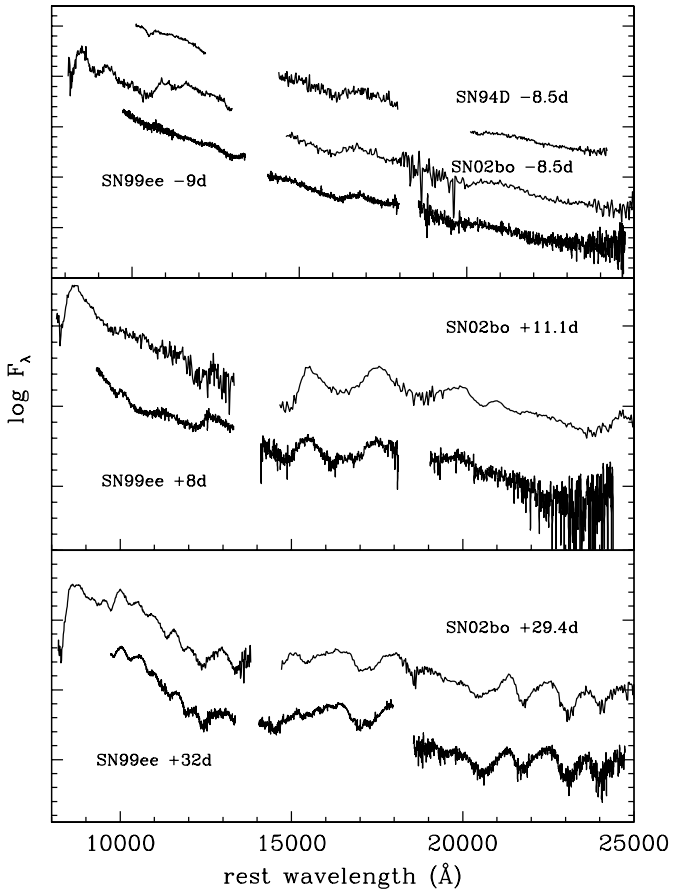

Figure 13. Comparison of SN 2002bo IR spectra with those of SN 1999ee (from Hamuy et al. 2002) and SN 1994D for epoch –8.5d (Meikle et al. 1996). The spectra have been corrected for the redshift of the parent galaxies.

code originally developed by Abbott & Lucy (1985) to treat multi-line transfer in the expanding envelopes of hot stars. This code was further developed and adapted to SNe by Mazzali & Lucy (1993), Lucy (1999), and Mazzali (2000). We briefly describe here the structure of the MC code. Details can be obtained from the references given above. The code uses as input a model of the explosion (density v. velocity), the emergent luminosity L, the epoch t (time since explosion), the estimated velocity of the photosphere v_{ph} and a set of abundances. These are treated as homogeneous above the momentary photosphere.

The code divides the SN envelope into a number of shells, with the thickness of each shell increasing as a function of radius. Velocity is a continuous function of radius. For SN ejecta we may assume homologous expansion, $v = r/t$, where r is the radius and t the time since the explosion. Density is rescaled according to the epoch. The temperature in the various shells is computed assuming radiative equilibrium. At a given epoch, temperature and density are treated as constant in each shell. The Sobolev approximation is adopted. Another basic assumption is that all the radioactive decay and fast-electron energy is deposited below a sharply-defined radius, the "photosphere"

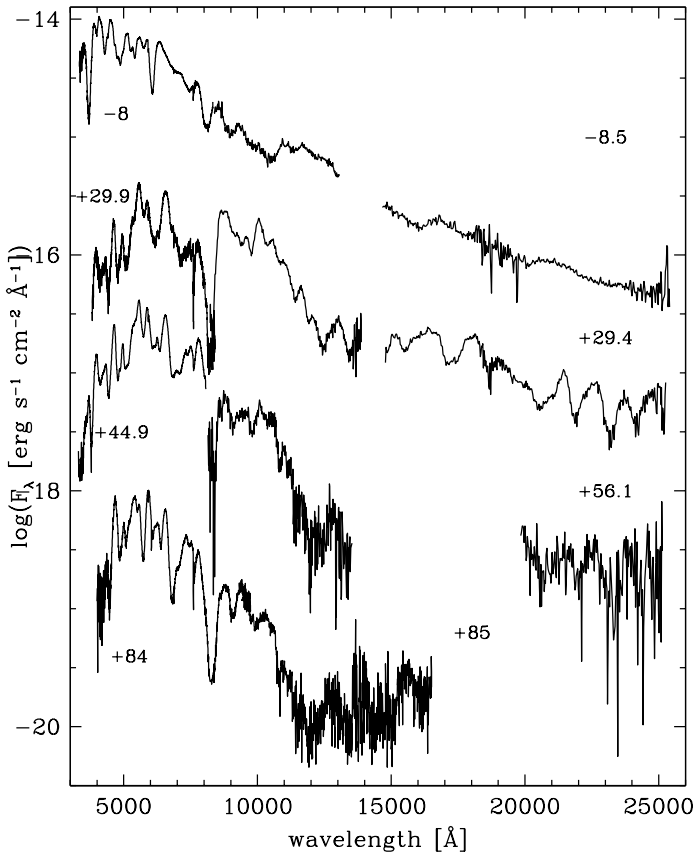

Figure 14. Opt-IR spectral evolution of SN 2002bo. Epoch from B maximum is given for each IR and optical spectra.

(Schuster-Schwarzschild approximation). This energy is distributed equally among packets, which represent "collective photons". These packets are characterised by a specific frequency, and their distribution with frequency represents the temperature at the photosphere. The packets propagate through the envelope (i.e. the ejecta above the photosphere) where they interact with electrons and atoms. Interaction with electrons is treated as scattering, while if a packet is absorbed by a line it is re-emitted in one of the allowed downward transitions. This is selected randomly, but weighted in proportion to the effective downward ($u \rightarrow l$) rate of each transition. The packet is assigned the new frequency and a random direction and the MC procedure continues until the packet either escapes the ejecta or is absorbed back in the photosphere. Finally, the emergent spectrum is computed using the formal integral (Lucy 1999).

Here, we present and discuss synthetic spectra for two epochs. In view of the somewhat unusual properties of SN 2002bo (e.g. the high velocity of several lines at early epochs), we computed models for the earliest spectrum (epoch $\sim$ −13 days) to determine whether or not the outer abundances are peculiar. We also computed models for a spectrum observed near maximum light in order to check the consistency of our results. The density structure and initial abundances were taken from the W7 model (Nomoto et al. 1984). However, unlike the W7 model, the composition is assumed to be uniform above the momentary photosphere. This is done by taking the W7 abundance at the velocity of the momentary photosphere and assuming that this is constant throughout the outer ejecta. This procedure is repeated for each epoch independently of the previous ones. An updated version of the code implementing the full stratified abundance distribution is in preparation. Keeping the density structure unchanged, the abundances were then adjusted to improve the model match to the data.

We consider first the earliest spectrum (–13 days). As indicated above, we started with a W7-like abundance distribution. For the envelope at this epoch, the W7 abundance is dominated by Oxygen (mass fraction of 65%) and a rather small contribution of Carbon (7%). IME are represented by Magnesium (8%), Silicon (10%), Sulphur (2%) and Calcium (2%). Iron group elements (Titanium and Chromium 0.5% each, 2% of Iron, 2% of Nickel and 1% of Cobalt) complete the initial abundance set. Note that in order to reproduce observed features an Fe abundance is adopted that is higher than the the W7 value. This is also higher than what ^{56}Co decay would allow, indicating that a significant quantity of Fe is left over from the progenitor. A grid of models were then computed in which radius of the "photosphere", emergent luminosity, abundance distribution, epoch and reddening were adjusted within a reasonable range to optimise the match to the observed –12.9 day spectrum. Each cell of the grid consists of a fixed epoch and reddening whilst the remaining parameters are consequently set to optimise the fit to the data. Although we could have included distance as one of the parameters of the grid, we chose to concentrate on a two parameter space to simplify our calculations. We therefore adopted a distance modulus $\mu = 31.67$, as given by the observations (Section 2.3). Spectra taken at the beginning of the rise of a SN are very useful to determine the correct epoch since luminosity changes significantly in this period. The position of the photosphere in velocity space can be determined fairly accurately by the position of the absorptions. Therefore, a change in the assumed epoch translates almost directly into a change of the photospheric radius ($R = vt$), which influences strongly the overall temperature structure and therefore the line depths and the ionization structure. The epoch was varied between 4 and 7 days post-explosion, and the reddening $E(B-V)$ between 0.00 and 0.45. Velocity and luminosity were adjusted to fit the overall flux level and the position of the absorptions. The best match spectrum is shown in Figure 15. The corresponding free parameter values obtained are: photospheric radius $= 6.67 \times 10^{14}$ cm (corresponding to $v_{ph} = 15,450$ km s^{-1}), log bolometric luminosity $log_{10}L = 41.94$ [erg s^{-1}], epoch $= 5 \pm 1$ days post-explosion, $E(B-V) = 0.30$ and a total mass of the envelope of $M_{tot} = 0.088$ M$_\odot$. The abundance distribution is discussed below. From this we deduce that the maximum-light spectrum corresponds to an epoch of 18 ± 1 days post-explosion, indicating a risetime in B of the same value. With a higher reddening of $E(B-V) = 0.45$, the best (but poorer) match (see Fig. 15) was achieved with radius $= 7.83 \times 10^{14}$ cm ($v_{ph} = 15,100$ km s^{-1}), $log_{10}L = 42.13$ [erg s^{-1}] at an epoch of 6 ± 1 days post-

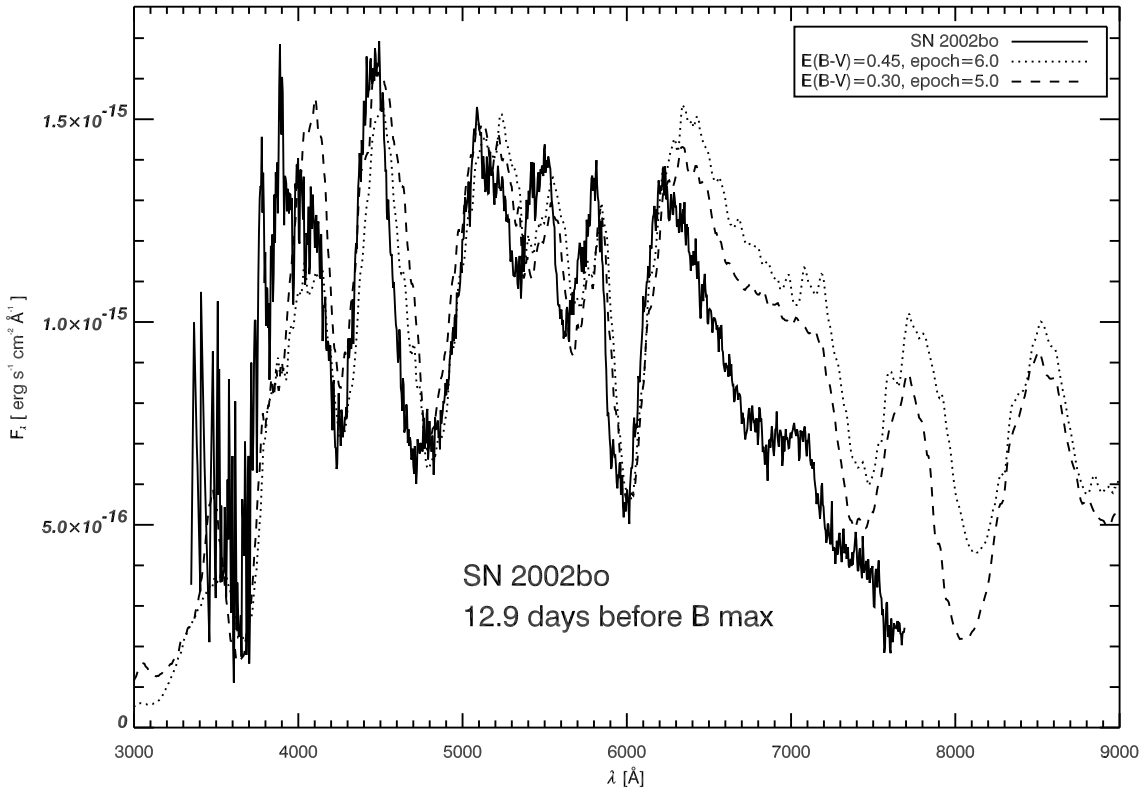

Figure 15. Spectrum of SN 2002bo 12.9 days before maximum. The dotted line shows the high reddened model with an epoch of 6.0 days after explosion and the dashed line represents the model with lower reddening at an epoch of 5.0 days after explosion.

explosion, implying a value of 19 ± 1 days for the epoch of the maximum-light spectrum and the rise time. The abundance distribution is discussed below. This higher-reddening match yields a luminosity which is closer to the value of $log_{10}L \approx 42.12$ [erg s^{-1}] inferred from Fig. 4 for this epoch, which could be expected, since the uvoir luminosity in fig 4 was derived using the larger reddening. If a smaller reddening was assumed, the SN luminosity would obviously be smaller, and comparable to that obtained from the low-reddening models here. While the overall best match was obtained with $E(B-V) = 0.30$, plausible matches were also obtainable with smaller reddening. However, since the photometry and NaID absorption indicate a higher value viz. $E(B-V) = 0.43 \pm 0.10$, we conservatively adopt $E(B-V) = 0.30 \pm 0.15$, and consider models with both $E(B-V) = 0.45$ and 0.30.

The radiation temperature at the photosphere T_R is found after six iterations determining the temperature structure in the envelope and counts for the "backwarming" effect, i.e. photons are scattered back into the photosphere and heat it up. The values are $T_R = 9420$ K for the low-reddening model and $T_R = 9710$ K for the high-reddening model. Since in this temperature region there are ionisation edges of some elements like Si and S, this difference in temperature affects the ionization structure and consequently the emergent spectra are significantly different. In the low-reddening case, the Ca abundance was reduced to 1/4 of its initial value while, for the high-reddening case, it was reduced to 1/10. All abundances of the iron group elements are significantly lower than in W7 ($\approx 10\%$ of the initial values), but the high-reddening model requires a higher Fe-group abundance in order to reproduce the observed strength of the FeII lines. This is due to the higher temperature in this model, which leads to a lower fraction of FeII. The overall reduction of most elements caused an increased oxygen abundance ($\geq 70\%$).

We now consider in detail the model matches to the early (–13 d) spectrum (Figure 15), and examine some of the more prominent features. Shortward of ∼6500 Å both models reproduce the main features of the data quite well. Starting at the bluest part of the spectrum, the need for a higher temperature in the high-reddening model is partly driven by the requirement to reproduce the total flux in this region. However this, in turn, tends to increase the ratio of doubly- to singly-ionised species. Consequently, to reproduce the deep MgII 4481 Å absorbtion at 4300 Å, a higher Mg abundance is required in the high-reddening model. A similar argument is relevant to the deep, broad absorption feature at ∼4800 Å, produced mostly by FeII lines. In the high-reddening model this requires an Fe abundance of 0.02 in the envelope, but in the low-reddening model this falls to 0.015. We conclude that higher abundances of Mg and Fe are required in the high-reddening model. In contrast, to reproduce the deep absorption feature at ∼5350 Å, attributed to SII 5640 Å, we need a somewhat higher S abundance in the *low*-reddening model (0.05 compared to 0.03). We ascribe this to a larger proportion of S recombining to the neutral state at this lower temperature compared with the high-reddening model. When we consider Si, a difficulty for the

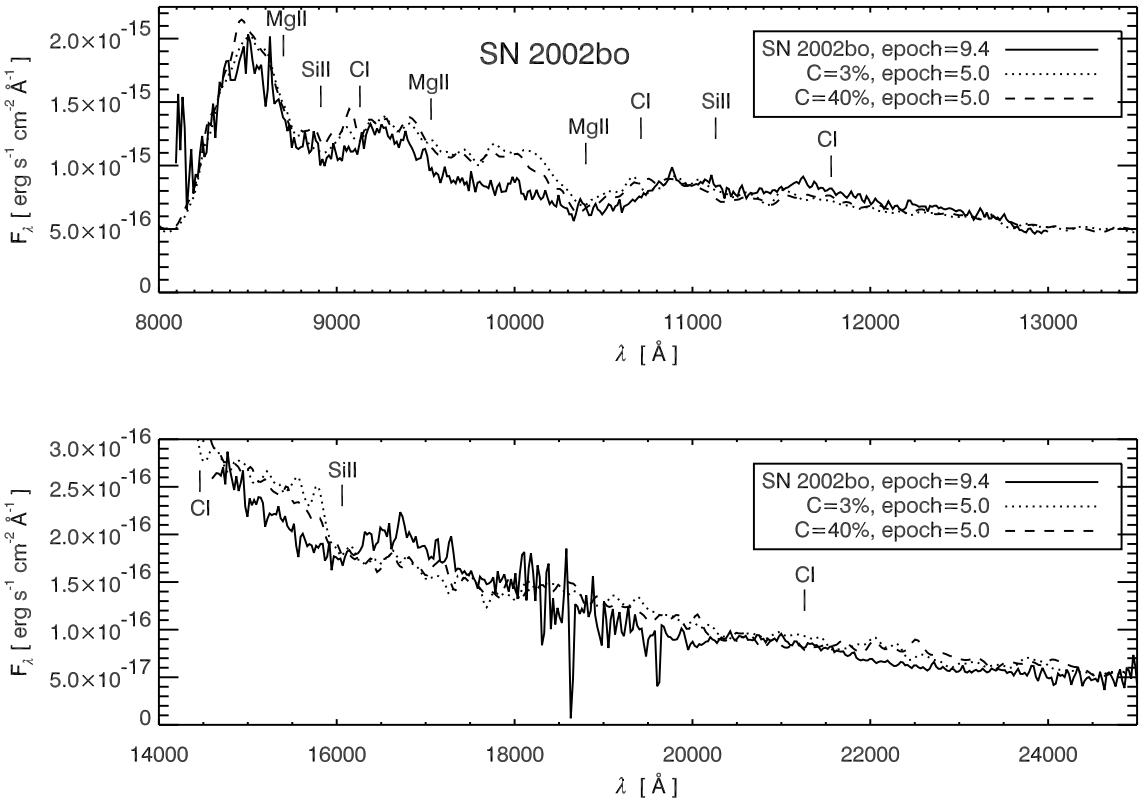

Figure 16. Near-infrared spectrum of SN2002bo. The –12.9 d model has been scaled to the flux level of the observations at day –8.5 before B_{max}. Also shown are two versions of the low-reddening spectral models with carbon abundances of 3% and 40% respectively (see text).

high-reddening model become apparent. In this model most of the Si is ionized to Si^{2+}, making it impossible to reproduce the full depth of the 5650 Å absorption, attributed to the SiII 5972 Å line. The low-reddening model is able to reproduce the absorption features due to SiII 5972 Å, 6355 Å, by invoking a relative Si abundance of 0.12 (mass fraction) at high velocities ($v \geq 15400$ km s^{-1}). W7 predicts no Si at such high velocities from which we may infer that extensive mixing has taken place. However, accepting this, we might also expect to see evidence of oxygen mixed downward to low velocities. That this is not observed in the later spectra perhaps suggests that O was at least partially burned to Si even in the outer layers.

At longer wavelengths, both models produce a large excess of flux. This is due to the limitation of the Schuster-Schwarzschild approximation which is used in the code. In the red/infrared part of the spectrum, where line opacity is low, the photosphere actually lies at a greater depth than is estimated in the code, and consequently the model overestimates the flux. Nevertheless, we have carried out a comparison of model spectra with the observations in the infrared region. Unfortunately there are no infrared observations available at day –12.9, when the spectral model is more applicable at such long wavelengths. The earliest IR-spectrum is from day –8.5. Therefore, in order to examine the 8000–25,000 Å region, we scaled the flux of the –12.9d low-reddening model by ×1.4 to bring it to the flux level of the observed spectrum from day –8.5. The IR spectrum is shown in Figure 16, together with the model spectra for two values of the carbon abundance (see below). In general there is reasonable agreement between the models and the observations with respect to the overall shape of the IR spectra. In the 8000–13000 Å window we identify features due to the MgII 9217,9243 Å doublet and the 10914,10915,10952 Å triplet. Additionally there is a SiII feature of minor importance at 9413 Å. In the 15,000–18,000 Å window we attribute the broad absorption at 16,000 Å in the figure to a blend of SiII 16,906 Å, 16,977 Å, 17,183 Å and MgII 16,760 Å, 16,800 Å, with the SiII feature dominating. Thus, at this early epoch we confirm the IR identifications proposed by Marion et al. (2003) for their spectra of other type Ia supernovae. Marion et al. (2003) point out that the Mg II IR features are valuable for placing limits on the mass of unburned material. We shall address this issue in a later paper. In the 20,000-25,000 Å region line no strong features were observed in the spectrum nor predicted by the model. There is only a shallow, broad P-Cygni feature at ∼20800Å which we attribute to SiII. Marion et al. (2003) did not cover this spectral region. A more detailed analysis of the red/infrared part of the spectrum will be accomplished in an upcoming paper using an improved version of the code.

One reason that early-time spectra are of particular interest is because, via the strength of CII lines in the red part of the spectrum, they can provide interesting limits on the amount of carbon present, and how far into the outer layers the burning penetrated. The carbon abundance at

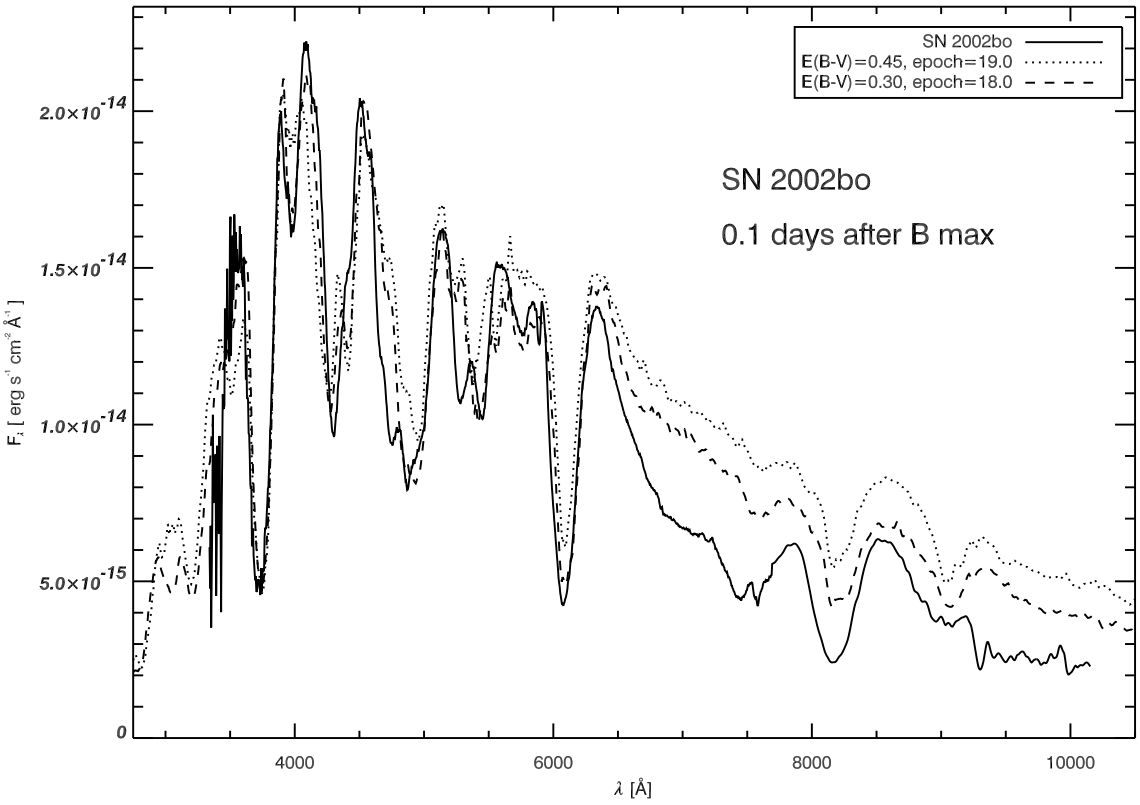

Figure 17. Spectrum of SN 2002bo 0.1 days after B maximum. Over-plotted are the two models with $E(B-V) = 0.45$ (dashed) and $E(B-V) = 0.30$ (dotted line).

extremely early times may even reveal the properties of the progenitor white dwarf. Fisher et al. (1997) suggested that the entire 'SiII' 6150 Å absorption feature in the –14 d spectrum of SN 1990N was actually CII 6578,83 Å at high velocity. However, Mazzali (2001) showed that this line could, at most, be responsible for only the red side of the 6150 Å feature, as indicated by its presence as a weak absorption at lower velocities sitting on top of the P-Cygni emission of the SiII line, and by the weakness of the corresponding CII 7231,36 Å line. Branch et al. (2003) identified absorption features due to CII 6578,83 Å and CII 7231,36 Å in the −9 d spectrum of SN 1998aq. They are also clearly visible in the −10 d spectrum of SN 1994D (Patat et al. (1996), Hernandez et al. (2000)), although by −8 d they had almost disappeared (see Fig. 6). However, in SN 2002bo there is no trace of these features, even in the earliest spectra. In order to place limits on the abundance of high velocity C implied by this negative observation, we increased the 7% carbon relative abundance specified by W7, to 40% throughout the envelope. This produced very strong CII 6578,83 Å features which were not present in the observed spectrum. We then decreased the carbon abundance until the CII 6578,83 Å features became fully undetectable in the synthetic spectrum. This occurred for a C abundance of 3%.

As a check, we extended the modelling to 25,000 Å where CI and CII lines are found in the model's line list. These include multiplets around 9,100 Å, 10,680 Å, 11,750 Å, 14,400 Å and 21,200 Å plus several single lines distributed throughout the 8000–25,000 Å region. Figure 16 shows the IR spectrum plus the 40% carbon and 3% carbon models. It can be seen that, even with a 40% carbon abundance, the carbon features are barely discernable. However, the observed spectrum shows no sign whatever of the predicted carbon features confirming that the carbon abundance is less than 40%. Reducing the carbon abundance to 3% causes the lines in the 8000–25,000 Å region to become too weak or too blended with other lines (mostly SiII or MgII) to be detectable. We conclude that the IR spectrum is consistent with a 3% carbon abundance, although the actual limit here is less stringent than in the optical region. We note that, aside from the low abundance, the weakness of the CI lines is due to the temperature of the SN ejecta which leads to an almost completely ionization to CII. The low carbon abundance is discussed in the next section.

We turn now to the optical spectrum taken close to maximum light (Fig. 17). By this epoch the photospheric radius has increased to 1.4×10^{15} cm (corresponding to $v_{ph} = 9000$ km s^{-1}) in the low reddening model, and $= 1.6 \times 10^{15}$ cm (corresponding to $v_{ph} = 9740$ km s^{-1}) in the high reddening model. The photospheric luminosities are 43.03 [erg s^{-1}] and 43.27 [erg s^{-1}] respectively. Once again the high-reddening model attains a higher radiation temperature ($T_R = 13420$ K) compared with the low-reddening model ($T_R = 12760$ K). Note that the temperature of the spectrum near peak brightness is hotter than at –13 days. Such behaviour was also observed in SN 1990N (Mazzali et al. 1993), one of the few other SNe Ia with very early spectral coverage. It is probably due to the fact that the heating coming from the delayed release of radiation, still overcomes the expansion cooling of the envelope.

Both models have a problem in reproducing the 4300–4500 Å absorption, which is dominated by SiII lines. To reproduce the depth of the absorption, we need a high Si abundance (62.1% for the higher reddening model and 66.7% for the lower reddening one, respectively) indicating that the part of the ejecta with velocities near 10,000 $\mathrm{km\,s^{-1}}$ is dominated by IME. As with the high-reddening model at the earlier epoch, the need for such a high abundance is driven by the fact that almost all the Si is doubly-ionised in the model. We also note that both models produce a double structure in the trough, with the high-reddening case being more pronounced. Curiously, while this structure is absent from SN 2002bo, it is present in SNe 1994D and 1998bu (Fig. 7). The persistence of a weak absorption due to SiIII 4567 Å in the model suggests that $E(B-V)$ could be even smaller than 0.30. The high ionisation also results in the absorption of the SiII 6355 Å line being slightly too shallow. However, most striking is the fact that the SiII 5958 Å absorption, while well reproduced in the low-reddening model is completely absent in the high reddening one.

As with the early-epoch spectrum, both models overproduce the flux longward of ∼6500 Å, with the high-reddening model being the most discrepant. The observed absorption at 7500 Å might be identifiable as OI 7771 Å. (Note that the narrower 7600 Å feature is the residual of the telluric absorption.) However, even with an unphysically high O abundance we cannot reproduce the depth of this feature since the high temperature ionises all the neutral oxygen. The modelled CaII absorption at ∼3750 Å due to the 3933,68 Å H&K doublet matches the observation very well, but the absorption at ∼8200 Å due to the ∼8500 Å IR triplet is too weak even after taking into account the offset between the spectral model and the observed continuum. Once again the match is somewhat better in the low-reddening model. In general, we find that the difficulties encountered by the high-reddening model are even larger at this epoch.

We conclude that modelling of both epochs suggests a reddening value smaller than the $\mathrm{E}(B-V) = 0.45$ derived from the Lira and NaID relations. This is indicated by the line ratios, line depths, overall shape of the spectra and the model abundances. Although distance was not included in our grid calculation, we computed some test models with high reddening and various distances for the –12.9 d spectrum. Relevant parameters are very sensitive to small changes at these early epoch (Mazzali & Schmidt 2000). We find that reasonable results can be obtained for a higher reddening, but this requires using a significantly shorter distance ($\mu \lesssim 31.00$). In order to keep a temperature similar to the low reddening model we need to use the same luminosity. This leads to a bolometric luminosity at maximum light of 43.00 [$\mathrm{erg\,s^{-1}}$], similar to the luminosity of the low reddening model (43.03 [$\mathrm{erg\,s^{-1}}$]). So the model-derived luminosity is in any case lower than the value 43.19 [$\mathrm{erg\,s^{-1}}$] suggested by the observations (Section 2.3). The spectral model-derived explosion epoch of -18 ± 1 days is consistent with the rise-time derived from our photometry using the Riess et al. (1999) procedure, and with the average value for SNe Ia given by Riess et al. It may be that some of the difficulties encountered with the model results presented here arise from the artificial homogenisation of the element distribution in the envelope. The distribution of the elements throughout the ejecta will be addressed in a separate analysis using an improved version of the MC code, including abundance stratification.

3 DISCUSSION

We have presented optical/near-infrared photometry and spectra of the type Ia SN 2002bo spanning epochs from –13 days before maximum B-band light to +102 days after. The pre-maximum optical coverage is particularly complete. The extinction deduced from the observed colour evolution and from interstellar NaID absorption is quite high viz. $\mathrm{E}(B-V) = 0.43 \pm 0.10$. On the other hand, model matches to the observed spectra point to a lower reddening ($\mathrm{E}(B-V) \sim 0.30$). We have been unable to resolve this reddening dichotomy. However, the ESC has monitored another supernova, SN 2002dj. This event exhibits photometric and spectroscopic similarities to SN 2002bo, but suffers from much less interstellar extinction. Modelling of the spectra of SN 2002dj (Pignata et al, in preparation) may help to establish the true extinction to SN 2002bo.

In some respects, SN 2002bo behaves as a typical "Branch normal" type Ia supernova (SN Ia) at optical and IR wavelengths. We find a B-band risetime of 17.9±0.5 days, a Δm_{15}(B) of 1.13 ± 0.05, a de-reddened $M_B = -19.41 \pm 0.42$, and a bolometric maximum of $\log L = 43.19$. However, comparison with other type Ia supernovae having similar Δm_{15}(B) values indicates that in other respects, SN 2002bo is unusual. The evolution of the SN 2002bo $(B-V)$ and $(V-R)$ colours shows some differences from that seen in SNe 1994D, 1998bu, 2001el (see Fig. 3). Moreover, while the optical spectra of SN 2002bo are very similar to those of SN 1984A (which has a similar Δm_{15}(B) = 1.19), lower velocities and a generally more structured appearance are found in SNe 1990N, 1994D and 1998bu (see also Hatano et al. 2000), whose values of Δm_{15}(B) are only slightly smaller (SNe 1990N and 1998bu) or slightly larger (SN 1994D). The evolution of $\mathcal{R}$(SiII) for SN 2002bo is strikingly different from that shown by other type Ia supernovae. The SN 2002bo spectra demonstrate the existence of S at 16,000 km/s, Si at $> 17,500$ km/s and Ca at $> 26,000$ km/s. While small amounts of primordial abundances may be present, this cannot explain the strength of the high velocity IME spectral features. Moreover, modelling of the SiII 5972, 6355Å lines confirms the presence of Si at velocities higher than that predicted by W7. We conclude that the behaviour of SN 2002bo cannot be easily related to a single parameter description of the properties of SNe Ia (see also Hatano et al. (2000)).

The presence of high-velocity IME (Si, S, Ca) in SN 2002bo (and SN 1984A) may be interpreted in various ways. One possibility is that the explosion that became SN 2002bo was more energetic than that of the average SN Ia, thus setting material in motion at higher velocities. Given that the velocities in SNe 2002bo and 1984A are about 20% higher than in normal SNe Ia, the kinetic energy of the explosion would have to be about 44% larger. However, these high velocities are shown only by the IME. In the iron-group layers the Fe nebular lines have velocities comparable to those of normal SNe Ia, although lying to the higher velocity side of the distribution. Therefore, the physical difference between SN 2002bo and more normal SNe may

not be so great. In support of this view, we note that most of the kinetic energy is produced by burning to Si, while the remaining burning stages to NSE make a further, but minor contribution.

Therefore one may imagine a situation where burning to IME continues further out into the outermost layers in SNe 2002bo and 1984A than in other SNe Ia. This enhanced burning may point to some form of delayed detonation (see also Lentz et al. (2001)). This scenario has some useful consequences. Since the IME are produced at high velocities, but at the same time no more ^{56}Ni is produced than in other SNe Ia, then this would only have a small effect on Δm_{15}, since the shape of the light curve depends mostly on the behaviour of the line opacity, which is dominated by Fe-group elements (Mazzali et al. 2001). Moreover, the amount of progenitor material (C, O) observed in the outer layers of the SN would be greatly reduced. In particular, if burning proceeded at a relatively low density, C, but not O, would be burned to IME thus explaining the unusually low abundance of carbon at the highest velocities. It may be that the –13 day photosphere happened to fall at the location where C but not O had been burned to IME. This layer has a small velocity extent, and its location depends on the overall properties of the explosion (it is located further out the more ^{56}Ni was synthesized, see e.g. Iwamoto et al., Fig 25). It is therefore possible that the original, high C abundance might still exist in layers well above the photosphere of the –13 day spectrum, although those layers may have densities too low for C lines to be strong once the photosphere has receded to deeper layers. Furthermore, this picture may explain the cool early-time temperatures indicated both by the pre-maximum Si II line ratio and by the SiIII 4553, 4568Å feature (see Sect.2.5). If Si extends to higher levels than normal, to velocities where unburned material is usually found, then such Si would be subject to a much-reduced γ-ray/fast-electron flux and its temperature would be lower than in the Si layer of more typical SNe Ia. There would be a number of observable consequences of this situation: 1) at very early times, the Si lines would be stronger than in other SNe, and would extend to higher velocities, 2) also at very early times, the Si line ratio would indicate a lower temperature than in other SNe, because the Si that contributes to the lines is located further from the ^{56}Ni, and 3) as time goes by it might be expected that the Si line ratio would evolve towards higher temperatures, as confirmed in Figure 9.

The above scenario will be more severely tested by spectral models which include abundance stratification, and by the acquisition of even earlier spectra. Extremely early observations may even place constraints on the progenitor composition. In addition, the reason for such behaviour will be explored via detailed 3D studies of the explosion, which are currently under way.

Other possible explanations exist for the atypical behaviour of SNe 2002bo and 1984A. For example, the IME produced at deeper layers may be more efficiently mixed upwards in SNe 2002bo and 1984A than in other SNe Ia. This may provide an equally plausible explanation for all the characteristics discussed above. One way to discriminate between the two possibilities is to look for C and O at lower velocities - if IME have been mixed out, C and O should have been mixed in.

A somewhat more exotic scenario is that SNe 2002bo and 1984A came from more massive progenitors, such as might be produced by a binary white-dwarf merger. In this case, however, one might expect that not only would more IME be produced at higher velocities, but also that more ^{56}Ni would be synthesised. This scenario would lead not only to broad Fe nebular lines in the late-time spectrum, but also to a brighter SN (Arnett 1982), something that does not seem to be the case here. The nebular lines in the late-time spectrum of SN 2002bo have widths comparable to those of other typical SNIa.

ACKNOWLEDGMENTS

We thank K. Krisciunas and N. Suntzeff for providing us with their JHK photometry of SN 2002bo prior to publication. We also thank J.C. Wheeler for providing us an unpublished spectrum of SN 1984A taken at McDonald Observatory. This work is supported in part by the European Community's Human Potential Programme under contract HPRN-CT-2002-00303, "The Physics of Type Ia Supernovae". This work is partially based on observations collected at the European Southern Observatory, Chile (ESO N^o 169.D-0670), the Italian Telescopio Nazionale Galileo (TNG), La Palma, the Isaac Newton (INT), Jacobus Kapteyn (JKT) and William Herschel (WHT) Telescopes of the Isaac Newton Group, La Palma, and the United Kingdom Infrared Telescope (UKIRT), Hawaii. The TNG is operated on the island of La Palma by the Centro Galileo Galilei of INAF (Istituto Nazionale di Astrofisica) at the Spanish Observatorio del Roque de los Muchachos of the Instituto de Astrofisica de Canarias. The INT, JKT and WHT are operated on the island of La Palma by the Isaac Newton Group (ING) in the Spanish Observatorio del Roque de los Muchachos of the Instituto de Astrofisica de Canarias. UKIRT is operated by the Joint Astronomy Centre on behalf of the U.K. Particle Physics and Astronomy Research Council. Some of the data reported here were obtained as part of the ING and UKIRT Service Programmes. Some observations were also done within the International Time Programme "Omega and Lambda from supernovae and the Physics of SNe Ia explosions" at La Palma. For the Nordic Optical Telescope (NOT) observations we thank J. Gorosabel, T. Grav, T. Dahlen and G. Östlin who gave up some of their observational time. The NOT is operated on the island of La Palma jointly by Denmark, Finland, Iceland, Norway, and Sweden, in the Spanish Observatorio del Roque de los Muchachos of the Instituto de Astrofisica de Canarias. This work has made use of the NASA/IPAC Extragalactic Database (NED) which is operated by the Jet Propulsion Laboratory, California Institute of Technology, under contract with the National Aeronautics and Space Administration. We have also made use of the Lyon-Meudon Extragalactic Database (LEDA), supplied by the LEDA team at the Centre de Recherche Astronomique de Lyon, Observatoire de Lyon.

REFERENCES

Altavilla G., Fiorentino G., Marconi M. et al., 2003, MNRAS, submitted

Abbott D.C., Lucy L.B., 1985, ApJ 288, 679

Arnett W. D., 1982, ApJ, 253, 785

Axelrod T.S., PhD. thesis, Univ. California at Santa Cruz

Barbon R., Rosino L., Iijima T., 1989, A&A, 220, 83

Barbon R., Benetti S., Rosino L., Cappellaro E., Turatto M., 1990, A&A, 237, 79

Benetti S., 1989, Thesis, University of Padua

Benetti S., Altavilla G., Pastorello A., Riello M., Turatto M., Cappellaro E., Tomov T., Mikolajewski M., 2002, IAUC, 7848, 3

Branch D., Drucker W., Jeffery D. J., 1988, ApJ, 330, L117

Branch D., Fisher A., Nugent P., 1993, AJ, 106, 2383

Branch D., Garnavich P., Matheson T., Baron E., Thomas R.C., Hatano K., Challis P., Jha S., Kirshner R.P., 2003, AJ, 126, 1489

Cacella P., Hirose Y., Nakano S., Kushida Y., Kushida R., Li W. D., 2002, IAUC, 7847

Caldwell R. R., Dave R., Steinhardt P. J., 1998, PhRvL, 80, 1582

Cardelli J.A., Clayton G.C. Mathis J.S., 1989, ApJ, 345, 245

Chornock R., Li W. D., Filippenko A. V., 2002, IAUC, 7851, 3

Contardo G., Leibundgut B., Vacca W.D., 2000, A&A, 359, 876

Fisher, A., Branch D., Nugent P., Baron, E., 1997, ApJ, 481, L89

Freedman W. L. et al., 2001, ApJ, 553, 47

Garcia A. M., 1993, A&AS, 100, 47

Gibson, B.K., Stetson P.B., Freedman W. L., et al., 2000, ApJ, 529, 723

Hamuy M., Maza J., Pinto P. A., et al., 2002, AJ, 124, 417

Hatano K., Branch D., Lentz E.J., Baron E., Filippenko A.V., Garnavich P.M., 2000, ApJ, 543, L49

Hernandez M., Meikle W.P.S., Aparicio A., et al., 2000, MNRAS, 319, 223

Hillebrandt W., Niemeyer J. C., 2000, ARA&A, 38, 191

Hunt L. K., Mannucci F., Testi L., Migliorini S., Stanga R. M., Baffa C., Lisi F., Vanzi L., 1998, AJ, 115, 2594

Iwamoto K., Brachwitz F., Nomoto K., Kishimoto N., Umeda H., Hix W. R., Thielemann F., 1999, ApJS, 125, 439

Jha S., Garnavich P. M., Kirshner R. P., et al., 1999, ApJS, 125, 73

Kawakita H., Kinugasa K., Ayani K., Yamaoka H., 2002, IAUC, 7848, 2

Krisciunas K., Suntzeff N. B., Candia P., et al., 2003, AJ, 125, 166

Landolt A. U., 1992, AJ, 104, 340

Leibundgut B., Tammann G. A., Cadonau R., Cerrito D., 1991a, A&AS, 89, 537

Leibundgut B., Kirshner R. P., Filippenko A. V., Shields J. C., Foltz C. B., Phillips M. M., Sonneborn G., 1991b, ApJ, 371, L23

Leibundgut B., Kirshner R. P., Phillips M. M., et al., 1993, AJ, 105, 301

Lentz E. J., Baron E., Branch D., Hauschildt P. H., Nugent P. E., 2000, ApJ, 530, 966

Lentz E. J., Baron E., Branch D., Hauschildt P.H., 2001, ApJ, 547, 402

Li W., Filippenko A. V., Gates E., et al., 2001, PASP, 113, 1178

Lira P., 1995, M.S. thesis, University of Chile

Lucy L.B., 1999, A&A 345, 21 1

Marion G.H., Höflich P., Vacca W.D., Wheeler J.C., 2003, ApJ, 591, 316

Matheson T., Jha S., Challis P., Kirshner R., Hradecky V., 2002, IAUC, 7849, 2

Mazzali P.A., Lucy L.B., 1993, A&A 279, 447 (Paper II)

Mazzali P.A., Lucy L., 1998, MNRAS, 295, 428

Mazzali P. A., Lucy L., Danziger I. J., Gouiffes, C., Cappellaro E., Turatto M., 1993, A&A, 269, 423

Mazzali P. A., Cappellaro E., Danziger I. J., Turatto M., Benetti S., 1998, ApJ, 499, L49

Mazzali P.A., 2000, A&A 363, 705

Mazzali P.A., Schmidt B.P., 2000, in: *New Cosmological Data and the Values of the Fundamental Parameter,* Proceedings of IAU Symposium no. 201, in press

Mazzali P. A., 2001, MNRAS, 321, 341

Mazzali P. A., Nomoto, K., Cappellaro E., Nakamura, T., Umeda, H., Iwamoto, K., 2001, ApJ, 547, 988

Meikle W. P. S., Cumming R. J., Geballe T. R., et al., 1996, MNRAS, 281, 263

Meikle W. P. S., 2000, MNRAS, 314, 782

Nobili S., Goobar A., Knop R., Nugent P., 2003, A&A, 404, 901

Nomoto K., Thielemann F.-K., Yokoi K., 1984, ApJ 286, 644

Nugent P., Phillips M., Baron E., Branch D., Hauschildt P., 1995, ApJ, 455, L147

Patat F., Benetti S., Cappellaro E., Danziger I. J., della Valle M., Mazzali P. A., Turatto M., 1996, MNRAS, 278, 111

Perlmutter S., Aldering G., Goldhaber G., et al., 1999, ApJ, 517, 565

Persson S. E., Murphy D. C., Krzeminski W., Roth M., Rieke M. J., 1998, AJ, 116, 2475

Phillips M. M., Lira P., Suntzeff N. B., Schommer R. A., Hamuy M., Maza J., 1999, AJ, 118, 1766

Riess A. G., Filippenko A. V., Challis P., et al., 1998, AJ, 116, 1009

Riess A. G., Filippenko A. V., Li W., et al., 1999, AJ, 118, 2675

Rigon L., Turatto M., Benetti S., et al., 2000, MNRAS, 340, 191

Saha A., Sandage A., Tammann G. A., Dolphin A. E., Christensen J., Panagia N., Macchetto F. D., 2001, ApJ, 562, 314

Sarneczky K., Bebesi Z., 2002, IAUC, 7863, 3

Schlegel D. J., Finkbeiner D. P., Davis M., 1998, ApJ, 500, 525

Spyromilio J., Pinto P. A., Eastman R. G., 1994, MNRAS, 266, L17.

Stritzinger M., Hamuy M., Suntzeff N. B., et al., 2002, AJ, 124, 2100

Suntzeff N. B., 1996, in IAU Colloq. 145: *Supernovae ans Supernovae Remnants*, eds. R. McCray, Z. Wang (Cambridge University Press), p.41

Suntzeff N. B., Phillips M. M., Covarrubias R., et al., 1999, AJ, 117, 1175

Suntzeff N. B., 2003, in the proceedings to the ESO/MPA/MPE Workshop (an ESO Astrophysics Symposium) *From Twilight to Highlight: The Physics of Supernovae*, eds. B. Leibundgut and W. Hillebrandt (Springer-Verlag), p.183

Tanvir, N. R., Ferguson, H. C., Shanks, T. 1999, MNRAS, 310, 175

Tonry J. L., Dressler A., Blakeslee J. P., Ajhar E. A., Fletcher A. B., Luppino G. A., Metzger M. R., Moore C. B., 2001, ApJ, 546, 681

Turatto M., Benetti S., Cappellaro E., Danziger I. J., della Valle M., Gouiffes C., Mazzali P. A., Patat F., 1996, MNRAS, 283, 1

Turatto M., Piemonte A., Benetti S., Cappellaro E., Mazzali P. A., Danziger I. J., Patat F., 1998, AJ, 116, 2431

Turatto M., Benetti S., Cappellaro E., 2003, in the proceedings to the ESO/MPA/MPE Workshop (an ESO Astrophysics Symposium) *From Twilight to Highlight: The Physics of Supernovae*, eds. B. Leibundgut and W. Hillebrandt (Springer-Verlag), p.200

Vacca W. D., Leibundgut B., 1996, ApJ, 471, L37

Wegner G., McMahan R.K., 1987, AJ, 93, 287

Wheeler J. C., Hoeflich P., Harkness R. P., Spyromilio J., 1998, ApJ, 496, 908